Chemical Geology 424 (2016) 30–50

Contents lists available at ScienceDirect

Chemical Geology

journal homepage: www.elsevier.com/locate/chemgeo

An assessment of monazite from the Itambé pegmatite district for use as U–Pb isotope reference material for microanalysis and implications for the origin of the "Moacyr" monazite

Guilherme O. Gonçalves [a,*], Cristiano Lana [a], Ricardo Scholz [a], Ian S. Buick [b], Axel Gerdes [c], Sandra L. Kamo [d], Fernando Corfu [e], Moacyr M. Marinho [f], Alexandre O. Chaves [g], Claudio Valeriano [h], Hermínio A. Nalini Jr. [a]

[a] Departamento de Geologia, Universidade Federal de Ouro Preto, Campus Morro do Cruzeiro s/n, 35430-000 Ouro Preto, MG, Brazil
[b] Department of Earth Sciences, Stellenbosch University, Private Bag X1, Stellenbosch, Matieland 7602, South Africa
[c] Institute of Geosciences, Goethe University, Altenhöferallee 1, Frankfurt am Main 60438, Germany
[d] Jack Satterly Geochronology Lab., Department of Earth Sciences, University of Toronto, Earth Sciences Centre, 22 Russell Street Toronto, M5S 3B1, Ontario, Canada
[e] Department of Geosciences, University of Oslo, Geologibygningen Sem Sælands vei 1, 0371, Oslo, Norway
[f] Departamento de Geologia, Instituto de Geociências, Universidade Federal da Bahia, Campus Ondina, Rua Barão de Jeremoabo, s/n, 40170-115 Salvador, BA, Brazil
[g] Departamento de Geologia, Instituto de Geociências, Universidade Federal de Minas Gerais, Av. Antônio Carlos n 6.627, Pampulha, 31270-901 Belo Horizonte, MG, Brazil
[h] Laboratório de Geocronologia e Isótopos Radiogênicos, Faculdade de Geologia, Universidade do Estado do Rio de Janeiro, Rua São Francisco Xavier 524/4006-A, Maracanã, 20559-900 Rio de Janeiro, RJ, Brazil

ARTICLE INFO

Article history:
Received 20 July 2015
Received in revised form 16 December 2015
Accepted 22 December 2015
Available online 31 December 2015

Keywords:
Bananeira monazite
Moacyr monazite
Reference material
U–Pb geochronology
Sm–Nd isotope composition
LA-ICP-MS
ID-TIMS
Araçuaí orogen
Eastern Brazillian pegmatite belt
Pegmatites

ABSTRACT

Large quantities of monazite from different pegmatite bodies of the Itambe pegmatite district were investigated to assess their suitability as U–Pb and Sm–Nd isotope reference materials for LA-ICP-MS and to track the origin of a piece of the Moacyr monazite (termed here Itambé), a widely used reference material for LA-ICP-MS U–Pb geochronology. Monazite from the largest pegmatite bodies in the district (the Bananeira, Coqueiro and Paraíso pegmatites) are Ce-monazite, with negligible amounts of the huttonite and brabantite components. They are homogeneous in major and trace elements, which makes them potential candidates as compositional reference materials. U–Pb LA-ICP-MS and ID-TIMS analyses yielded identical ages within error. Although the ID-TIMS ages (507.7 ± 1.3 ($^{207}Pb^*/^{235}U$) and 513.6 ± 1.2 Ma ($^{206}Pb^*/^{238}U$)) were reversely discordant, spot ages determined by LA-ICP-MS geochronology were concordant at ca 508 Ma. The Bananeiro monazite was assessed as a LA-ICP-MS U–Pb primary reference material against other known reference materials (treated as unknowns). This approach successfully reproduced the previously published ages of the reference materials. MREE/HREE fractionation (ie, $(La/Gd)_N$ and $(Gd/Lu)_N$ values), Eu/Eu^* and the chondrite-normalized REE patterns suggest that the "Itambé" monazite aliquot is very similar to that from the Coqueiro pegmatite. This similarity is likewise apparent in their Sm–Nd isotope compositions. Moreover, the εNdi values of the "Itambé" monazite fragment (εNdi = −4.2) and those from all the major pegmatites in the district, are distinct from other reference materials (eg, Managountry; εNdi = −22.3) as well as gem-quality monazite from c. 490–520 Ma pegmatites from the Araçuaí Orogen, further to the south. The εNdi can provide a further distinction for tracing Brazillian gem-quality monazite reference materials.

1. Introduction

Monazite (Ce, La, Nd, Th) PO_4 is a monoclinic light rare earth element (LREE; Ni et al., 1995) orthophosphate, with a general formula given by ABO_4, where A = Bi, Ca, Ce, La, Nd, Th, U and B = As, P, Si (Back and Mandarino, 2008). Due to its high concentration of U (hundreds to thousands ppm) and Th commonly >50,000 ppm (Parrish, 1990, Heaman and Parrish, 1991) and low concentrations of common Pb, monazite has proven useful for constraining the timing of geological events using U–Th–Pb geochronology (Hawkins and Bowring, 1997; Kosler et al., 2001; Harrison et al., 2002; Williams et al., 2007, Kohn and Vervoort, 2008; Warren et al., 2011; Goudie et al., 2014). In addition, owing to its high concentration of Sm and Nd (e.g., ~10^4 to 10^5 ppm; Tomascak et al., 1998; McFarlane and McCulloch, 2007), monazite has also been shown to be useful for isotopic tracing because the original Sm–Nd isotopic composition of the source rock may be preserved despite high-temperature overprinting (Rapp and Watson, 1986; Montel and Seydoux, 1998; Hammerli et al., 2014). Clearly, the combination of U–Th–Pb ages, Sm–Nd isotope compositions and chemical composition variation of monazite provides a powerful tool for

* Corresponding author at: Departamento de Geologia, Universidade Federal de Ouro Preto, Ouro Preto, MG 35430000, Brazil.
E-mail address: oliveira.geologo@gmail.com (G.O. Gonçalves).

http://dx.doi.org/10.1016/j.chemgeo.2015.12.019
0009-2541/

studying crustal evolution (McFarlane and McCulloch, 2007; Thöni et al., 2008; Gregory et al., 2009).

Monazite has a high closure temperature for Pb (> 900 °C; Cherniak et al., 2004; Gardes et al., 2006), which means that the diffusion of this cation is negligible, even at high-grade conditions (e.g., Cherniak et al., 2004; Gardes et al., 2006). The low diffusivity of major and trace elements also allows the preservation of compositional domains that can record the geological processes that have influenced the host rock (Foster et al., 2000, 2002; Catlos et al., 2002; Williams et al., 2007), e.g., sub-solidus vs. suprasolidus growth in polymetmorphosed metapelitic rocks (Buick et al., 2010). One disadvantage of using monazite for U–Th–Pb dating is its ability to recrystallize under the presence of fluid, potentially causing resetting of the U–Th–Pb system (Harlov et al., 2011; Williams et al., 2011).

Sm–Nd isotope systematics in monazite resides in the fact that those elements are relatively immobile (DePaolo, 1988) and that the chemical similarities of Sm–Nd makes the ratio of the two elements difficult to fractionate during most crustal processes (Rapp and Watson, 1986; Montel and Seydoux, 1998; Goudie et al., 2014). Moreover, the very high partition coefficients for those elements in monazite make the system difficult to reset (Stepanov et al., 2012). Recently, Sm–Nd isotopic analyses on monazite have been successfully undertaken by laser ablation-multicollector-inductively plasma-mass spectrometry (LA-MC-ICP-MS; McFarlane and McCulloch, 2007; Yang et al., 2008; Fisher et al., 2011; Iizuka et al., 2011; Liu et al., 2012), greatly improving the use of this systematics due to high-spatial resolution, fast data acquisition and low cost, in comparison to solution techniques.

The complex chemical and age zonation commonly preserved in individual monazite grains requires high spatial resolution analytical techniques, such as secondary ionization ion mass spectrometry (SIMS; Harrison et al., 1995; Stern and Berman, 2001), laser ablation-inductively coupled plasma-mass spectrometry (LA-ICP-MS; Machado and Gauthier, 1996; Poitrasson et al., 2000; Kosler et al., 2001; Horstwood et al., 2003; Gehrels et al., 2008; Paquette and Tiepolo, 2007; Kohn and Vervoort, 2008; Liu et al., 2012; Goudie et al., 2014) or electron probe microanalysis (EPMA; Suzuki and Adachi, 1991; Montel et al., 1996; Catlos et al., 2002, Williams et al., 2007). Although the three techniques require well-calibrated primary and secondary (quality control) reference materials, LA-ICP-MS has shown both the greatest increase in application to geochronology and isotope geochemistry, but is the most inherently destructive technique; it requires a constant supply of well-characterized reference materials in order to correct mass bias, elemental fractionation and instrumental drift. In general, relatively few U–Pb or Sm–Nd isotope reference materials are available for international distribution to high spatial resolution instruments and, of these, only a small subset have been distributed widely to LA-ICP-MS laboratories because only small amounts of the reference material are available and the destructive nature of the LA-based technique. Facilities otherwise develop in-house reference materials that are not widely available. For the case of LA-ICP-MS, the most commonly distributed U–Pb reference material is 44,069 monazite (c. 425 Ma - Aleinikoff et al., 2006), and Managountry monazite (Paquette et al., 1994) is also commonly used. Managountry monazite (Liu et al., 2012), Namaqualand monazite (also known as Steenkampskraal) (Liu et al., 2012) and 16-F-16 monazite (Iizuka et al., 2011) have all been proposed as reference materials for Sm–Nd isotope tracing.

One widely distributed reference material used for LA-ICP-MS or SIMS U–Pb geochronology and EPMA chemical dating comes from the Itambé pegmatite district of Bahia State (E Brazil; Silva et al., 1996; Fig. 1). Monazite from this source is described as either “Moacyr” or “Moacir” monazite in the literature (e.g. Seydoux-Guillaume et al., 1999, 2002; Paquette and Tiepolo, 2007; Dumond et al., 2008; Kohn and Vervoort, 2008; Gasquet et al., 2010; Palin et al., 2013; Harley and Nandakumar, 2014), but the exact location of those monazite crystals remains unclear. An initial TIMS age determination suggested that this monazite was concordant at c. 474 Ma (Seydoux-Guillaume et al., 1999). Subsequent TIMS age determinations have suggested that the Moacyr monazite is reversely discordant, with best-estimate crystallization ($^{207}Pb/^{235}U$) ages in the range c. 504–508 Ma (unpublished data quoted in Dumond et al., 2008, and Kohn and Vervoort, 2008; published data in Gasquet et al., 2010). The TIMS $^{207}Pb/^{235}U$ crystallization age estimates for Moacyr monazite do not entirely overlap, within error, and it is unclear whether this is an inter-laboratory analytical effect, or other unknown factor i.e. different sources. Compounding this uncertainty is the fact the Itambé pegmatite district contains three different large pegmatite bodies (the Bananeira, Coqueiro and Paraíso pegmatites; Fig. 2), all of which contain large quantities of monazite.

The main goal of this study is to assess the suitability of the monazites from the Itambe district as reference material for U–Pb geochronology. We furthermore attempt to identify the origin of a c. 50 g crystal fragment of Moacyr monazite (termed hereafter Itambé) that has previously been proposed as a SIMS oxygen isotope reference material by Rubatto et al. (2014) and its origin has been investigated by comparing new data on its age, Nd-isotope composition and chemical composition with those of monazite sampled for this study.

2. Sample description and geological setting

The Itambé pegmatite district occurs in the northernmost portion of the Eastern Brazilian Pegmatite Province (EBPP), a NNE-SSW belt of approximately 150,000 km^2. The EBPP consists of pegmatites that were

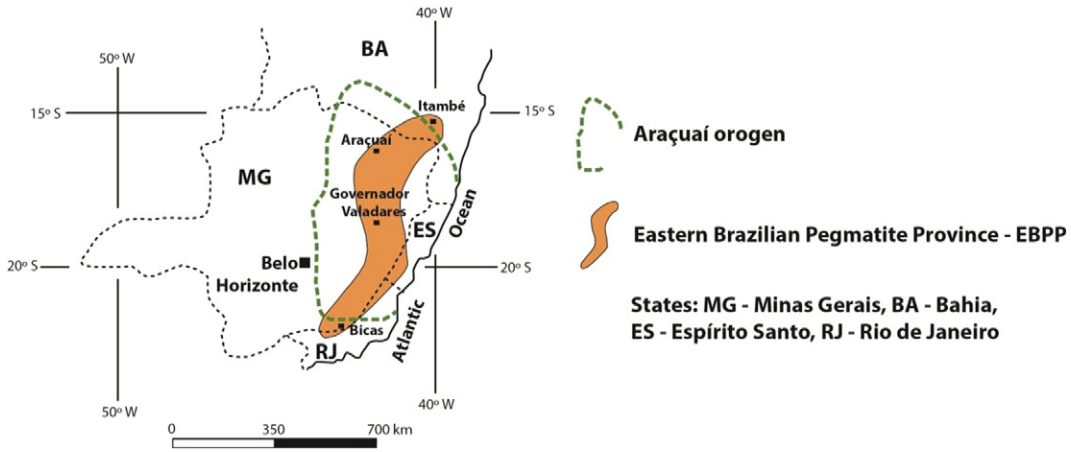

Fig. 1. Position of the Itambé pegmatite district, the northern tip of the Eastern Brazilian Pegmatite Province—EBPP, in relation to the Araçuaí orogen.

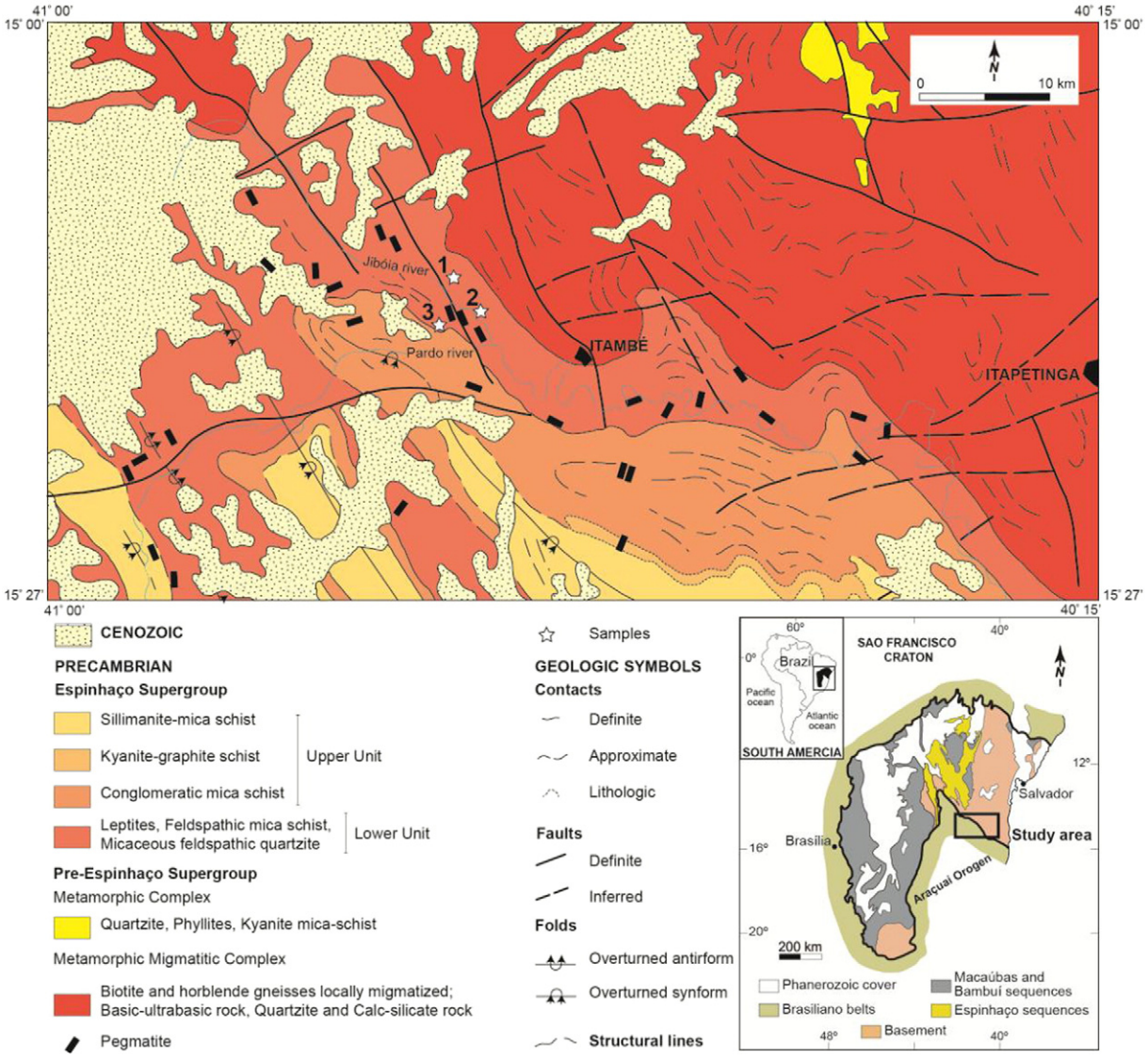

Fig. 2. Location of the Itambé pegmatite district in relation to the Aracuaí belt-São Francisco Craton (black square). The Itambé district geological map in detail is provided. The white stars are the Bananeira pegmatite body (1), Coqueiro (2) and Paraíso (3).
Modified from Silva et al. (1996).

mostly derived from highly-fractionated, late Neoproterozoic to Ordovician granitoids emplaced during the protracted evolution of the Araçuaí Orogen (AO) (Pedrosa-Soares et al., 2011). The Araçuaí Orogen occurs between the Archean–Paleoproterozoic São Francisco craton and the Atlantic shore (Pedrosa-Soares et al., 2001, 2008; Fig. 2).

The Itambé pegmatite district (Bahia State, eastern Brazil, Figs. 1 and 2) differs from those from the rest of the EBPP in that the pegmatites are located outside the Araçuaí orogen, in the transition zone between the São Francisco Craton and the orogen itself (Silva et al., 1996; Pedrosa-Soares et al., 2011). The district comprises three main pegmatite bodies: Bananeira, Coqueiro and Paraíso (Silva et al., 1996). The pegmatites of the Itambé district occurs mainly within feldspathic mica schists at the base of the Lower Unit of the Espinhaço Supergroup, a metasedimentary sequence of the Brasiliano Cycle (Silva et al., 1996). A more detailed description of the pegmatite bodies can be found on the Supplementary material. It is important to state that no record of granitoids, which could potentially be the source of the pegmatites, are present in the area (see Discussion).

Table 1
LA-Q-ICP-MS operating conditions and data acquisition parameters.

Instrument parameters					
ICP-MS		Laser		Analytical protocol	
Model	Agilent 7700×	Model	New wave UP213	Acquisition mode	Time resolved analysis
Forward power	1550 W	wavelenght	213 nm	Scanning mode	Peak jumping
Plasma gas (Ar)	15.0 L/min	Mode	Q-switched	Background acquisition time	20 s
Carrier gas (He)	0.96 L/min	Repetition rate	10 Hz	Signal acquisition time	40 s
Make up gas (Ar)	0.01 L/min	Focus	Sample surface	Wash-out time	20 s
		Spot size	25 μm	Isotopes determined	^{206}Pb, ^{207}Pb, ^{208}Pb, ^{232}Th, ^{238}U
		Energy density	~3 J/cm^2	Dwell time per isotope (ms)	10, 30, 10, 10, 15

Table 2
LA-SF-ICP-MS operating conditions and data acquisition parameters.

Instrument parameters					
ICP-MS		Laser		Analytical Protocol	
Model	Element II	Model	CETAC Nd:YAG	Acquisition mode	Time resolved analysis
Forward power	1200 W	Wavelenght	213 nm	Scanning mode	Peak jumping
Plasma gas (Ar)	0.8 L/min	Mode	E-scan	Background acquisition time	30 s
Auxiliary gas (Ar)	0.8 L/min	Repetition rate	10 Hz	Signal acquisition time	60 s
Carrier gas (He)	0.8 L/min	Focus	Sample surface	Wash-out time	20 s
Make up gas (Ar)	0.8 L/min	Spot size	15 μm	Scanned masses	202, 204, 206, 207, 208, 235, 232, 238
		Energy density	~5.6 J/cm2	Dwell time (ms)	4 ms
		Burst count	275	Mass resolution	300

Table 3
Faraday cup configuration and instrument operating parameters for Nd isotopic analysis.

Faraday cup configuration									
Cups	L4	L3	L2	L1	Center	H1	H2	H3	H4
Nominal mass	142	143	144	145	146	147	148	149	150
Measured elements	Nd	Nd	Nd	Nd	Nd	Sm	Nd	Sm	Nd
Natural abundance (%)	27.20	12.20	23.80	8.30	17.20	14.99	5.7	13.82	5.6
Interfering elements	Ce		Sm				Sm		Sm
Natural abundance (%)	11.11		3.07				11.24		7.38

Instrument parameters			
Thermo-Finnigan Neptune	MC-ICP-MS	Photon Machine 193 nm HelFx Excimer	
RF forward power	1200 W	Fluence	~4 J/cm^2
Cooling gas	15.5 L/min	Output power	~30 mJ
Auxiliary gas	0.85 L/min	Spot size	20 um
Sample gas	1.013 L/min	Pulse rate	8 Hz
Mass resolution	400 (Low)	He gas cell	1.2 L/min
Integration time	0.524 s		
Sensitivity on ^{146}Nd	15 V/ppm		
Acceleration voltage	10 kV		

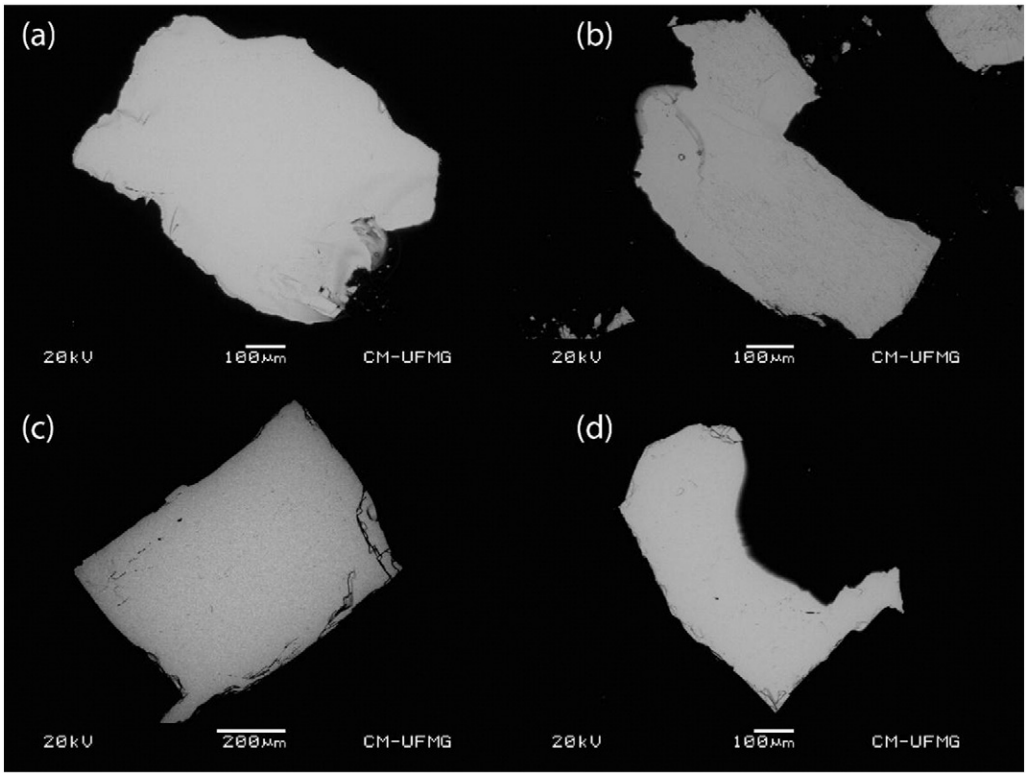

Fig. 3. Back-scattered electron (BSE) images of the studied monazites. (a) Bananeira, (b) Coqueiro, (c) Paraíso and (d) Itambé.

Table 4
Summary of the electron microprobe results. The oxide concentrations for each sample are the average of 12 EPMA point analyses. The complete dataset can be found in Supplementary material.The structural formula is calculated on the basis of four oxygens and the mole fractions are for the end-members Ce-monazite, huttonite and brabantite.

Sample	Bananeira	SD	Coqueiro	SD	Paraíso	SD	Itambé	SD
(%) CaO	0.92	0.01	0.93	0.02	0.44	0.01	0.69	0.01
SiO_2	0.94	0.05	1.37	0.07	1.64	0.05	1.11	0.09
MnO	0.03	0.01	0.02	0.01	0.02	0.01	0.03	0.01
FeO	0.01	0.01	0.01	0.01	0.01	0.01	<0.01	0.01
P_2O_5	28.50	0.23	27.66	0.31	27.34	0.25	28.14	0.20
PbO	0.17	0.01	0.21	0.01	0.18	0.01	0.16	0.01
Y_2O_3	1.56	0.02	0.41	0.03	0.77	0.04	0.40	0.04
ThO_2	7.03	0.05	8.45	0.27	8.05	0.06	6.79	0.20
UO_2	0.45	0.01	0.43	0.02	0.23	0.02	0.34	0.02
La_2O_3	9.92	0.10	11.74	0.13	12.74	0.09	11.75	0.18
Ce_2O_3	28.63	0.34	30.01	0.24	31.72	0.29	31.22	0.35
Pr_2O_3	3.21	0.09	3.13	0.09	3.20	0.07	3.37	0.09
Nd_2O_3	11.18	0.31	10.33	0.26	10.59	0.30	10.97	0.24
Sm_2O_3	5.48	0.12	4.02	0.15	2.66	0.08	4.13	0.15
Gd_2O_3	2.62	0.07	1.55	0.07	0.99	0.06	1.51	0.08
Dy_2O_3	0.54	0.06	0.41	0.08	0.25	0.06	0.35	0.04
Total	101.20		100.68		100.83		100.94	
Th/U	15.52		19.63		34.74		20.00	
(a.p.f.u.) Ca^{2+}	0.039		0.040		0.019		0.029	
Si^{4+}	0.037		0.055		0.066		0.044	
Mn^{4+}	0.001		0.001		0.001		0.001	
FeO	0.000		0.000		0.000		0.000	
P^{4+}	0.951		0.935		0.925		0.946	
Pb^{2+}	0.009		0.010		0.009		0.008	
Y^{3+}	0.033		0.009		0.016		0.008	
Th^{4+}	0.063		0.077		0.073		0.061	
U^{4+}	0.004		0.004		0.002		0.003	
$La3^{+}$	0.144		0.173		0.188		0.172	
Ce^{3+}	0.413		0.439		0.464		0.454	
Pr^{3+}	0.046		0.046		0.047		0.049	
Nd^{3+}	0.157		0.147		0.151		0.156	
Sm^{3+}	0.074		0.055		0.037		0.056	
Gd^{3+}	0.034		0.020		0.013		0.020	
Dy^{3+}	0.007		0.005		0.003		0.004	
TOTAL	2.01		2.02		2.01		2.01	
O^{2-}	4		4		4		4	
Mole fractions								
$ThSiO_4$	0.037		0.051		0.065		0.043	
$(La\text{-}Sm)PO_4$	0.816		0.839		0.867		0.868	
$(Th,Ca,U,Pb)[PO4]_2$	0.078		0.078		0.037		0.058	
Sum	0.932		0.967		0.970		0.969	

Monazite from the three pegmatites locally occurs as crystals in excess of 5 cm in diameter. Hand specimens of this monazite (and the Itambé crystal fragment) are deep red-orange in colour, and small fragments (100 s μm diameter shards) are orange-yellow. As noted previously, the origin of the Itambé crystal fragment is unclear and it might have come from any one of the three pegmatite bodies described above.

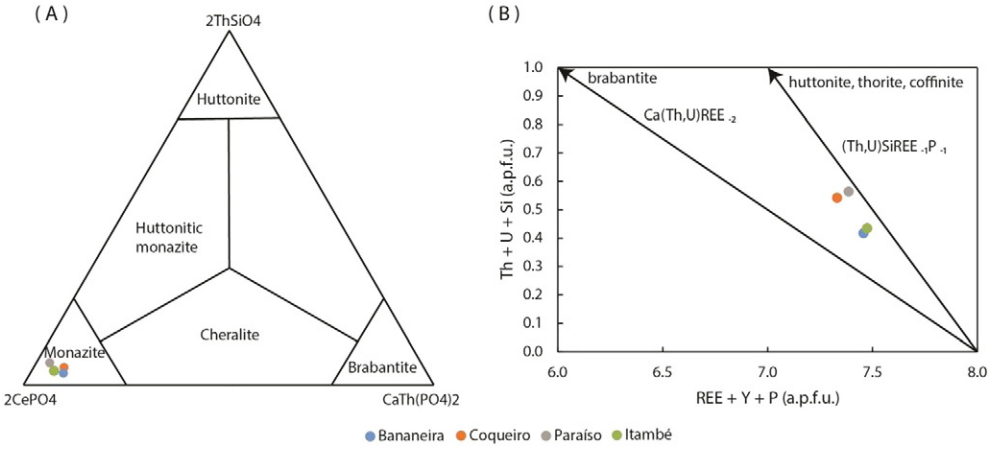

Fig. 4. (A) Nomenclature of the system $2CePO_4$–$CaTh(PO_4)_2$–$2ThSiO_4$ (Bowie and Horne, 1953; Förster, 1998). In calculating end-member proportions, on the basis of 4 oxygen atoms, the contents of other REE and Y are added to Ce, and the contents of U and Pb are included with the brabantite molecule. (B) Diagram (U + Th + Si) versus (REE + P + Y) (a.p.f.u) of formula proportions calculated on the basis of 16 oxygens atoms (Franz et al., 1996), that shows the different substitutions in monazite.

3. Sample preparation and analytical methods

Major and trace element chemical compositions, U–Pb ages and Sm–Nd isotopic compositions were determined on a number of different materials: 1) fragments of the Itambé SIMS oxygen isotope reference material (i.e., Rubatto et al., 2014); 2) monazite collected directly from the Bananeira and Coqueiro pegmatites; and 3) ~50 g crystal fragment of monazite from the Paraíso pegmatite, supplied by one of the authors (M.M.).

For each sample, random shards of large (>3 cm^3) crystals were carefully selected in order to obtain the most translucent material possible, free of inclusions or obvious zones of alteration. Those fragments were mounted on a double-sided tape, cast in 2.5 cm epoxy resin discs and subsequently polished to expose the fragments and obtain a flat surface that is suitable to backscattered electron (BSE) imaging and LA-ICP-MS analyses at the Isotope Laboratory, Universidade Federal de Ouro Preto. Small aliquots of the most concordant crystal and the Itambé monazite were separated for U–Pb ID-TIMS.

3.1. Chemical characterization

3.1.1. Electron microprobe

The mineral composition of the monazite aliquots were determined at the Centro de Microscopia at the Universidade Federal de Minas Gerais (UFMG, Belo Horizonte, Brazil) using a JEOL JXA-8900 electron microprobe equipped with a wavelength-dispersive system (WDS). Operating conditions, acquisition parameters, calibration procedures and data processing details can be found in the Supplementary material.

3.1.2. LA-Q-ICP-MS

Mineral composition were also determined by quadrupole laser ablation ICP-MS (LA-Q-ICP-MS) at the Laboratório de Geoquímica Ambiental (LGqA) in Universidade Federal de Ouro Preto (Minas Gerais, Brazil). An Agilent 7700× Q-ICP-MS coupled to a 213 NdYAG solid state laser (New Wave Research UP-213) was used. Average Ce (determined by EPMA) was used as internal reference material. Further details can be found in Supplementary material.

3.2. Isotopic characterization

3.2.1. LA-Q-ICP-MS

LA-Q-ICP-MS was used to determinate preliminary U–Pb ages. The samples with the best results in this stage were selected for further investigations. The U–Pb ages were acquired at the Laboratório de Geoquímica Ambiental (LGqA) in Universidade Federal de Ouro Preto using a Agilent 7700× quadrupole ICP-MS coupled to a 213 Nd:YAG laser (New Wave Research UP-213 nm). Laser and operation conditions and data acquisition parameters can be found on Table 1. The USGS 44069 monazite (Aleinikoff et al., 2006) was used as primary reference material. Concordia ages are reported with 2σ errors and weighted average ages and isotope ratios are reported at the 95% confidence level. Supplementary information on the methodology are presented in Supplementary material.

3.2.2. LA-SF-ICP-MS

The U–Pb ages were acquired at the Laboratório de Geoquímica Isotópica in Universidade Federal de Ouro Preto using a Thermo-Finnigan Element II, single collector sector field (SF) ICP-MS, coupled to a CETAC UV Nd:YAG 213 nm laser with a Helix ablation cell. Instrumental and acquisition parameters as shown in Table 2. Raw data were processed offline using an Excel® spreadsheet, following Gerdes and Zeh (2006, 2009). The 44,069 monazite (Aleinikoff et al., 2006) was used as primary reference material. All reported uncertainties (2σ) are propagated by quadratic addition of the external reproducibility (2 s.d.) obtained from the reference material 44,069 monazite during the analytical session and the within-run precision of each analysis

Table 5
Trace elements average absolute concentrations of the studied monazites. The complete dataset can be found in Supplementary material. Concentrations given in ppm.

Sample	^{29}Si	^{139}La	^{140}Ce	^{141}Pr	^{143}Nd	^{147}Sm	^{151}Eu	^{157}Gd	^{159}Tb	^{163}Dy	^{165}Ho	^{166}Er	^{169}Tm	^{174}Yb	^{175}Lu	^{178}Hf	^{206}Pb	^{232}Th	^{238}U	Eu/Eu^*	$((La/Gd)_N$	$((Gd/Lu)_N$
Bananeira	5709	120,774	233,074	27,814	96,710	19,578	366	9240	831	2817	273	483	55.9	289	27.3	0.115	243	68,252	972	0.07	11.43	42.14
SD	430	1644	0.008	240	1354	646	14.5	422	48.4	194	20.9	40.7	5.24	28.9	2.86	0.012	39.5	5574	179			
RSD%	7.5	1.4	0.0	0.9	1.4	3.3	4.0	4.6	5.8	6.9	7.6	8.4	9.4	10.0	10.5	10.8	16.3	8.2	18.5			
Coqueiro	7733	119,252	244,308	30,887	104,679	32,173	224	15,365	1499	3815	215	212	15.5	49.4	3.40	0.277	775	102,874	3093	0.03	6.74	558.73
SD	304	643	0.013	174	997	403	3.26	232	27.9	106	4.80	5.33	0.423	1.43	0.133	0.028	19.4	2699	106			
RSD%	3.9	0.5	0.0	0.6	1.0	1.3	1.5	1.5	1.9	2.8	2.2	2.5	2.7	2.9	3.9	10.3	2.5	2.6	3.4			
Paraíso	4609	115,176	258,229	33,980	123,589	53,670	123	32,109	3033	7051	351	318	20.9	67.6	4.82	0.311	945	83,005	3748	0.01	3.13	821.99
SD	727	2342	0.012	471	3450	2434	6.45	1867	195	472	24.1	21.1	1.34	3.93	0.294	0.035	64.8	7868	272			
RSD%	15.8	2.0	0.0	1.4	2.8	4.5	5.2	5.8	6.4	6.7	6.9	6.6	6.4	5.8	6.1	11.2	6.9	9.5	7.2			
Itambé	6003	123,677	254,159	31,539	108,324	35,148	228	16,991	1699	4213	233	235	18.1	64.3	4.08	0.158	644	88,546	2607	0.03	6.30	505.79
SD	330	2331	0.015	381	2337	1136	12.9	653	65.3	238	28.5	60.7	7.87	37.8	2.67	0.016	121	3603	479			
RSD%	5.5	1.9	0.0	1.2	2.2	3.2	5.7	3.8	3.8	5.7	12.2	25.8	43.5	58.8	65.4	10.4	18.8	4.1	18.4			
NIST	335,988	35.8	38.4	37.2	35.3	36.7	34.5	37.0	35.9	36.0	37.9	37.5	37.6	40.0	37.7	34.8	39.0	37.3	37.2	2.83	0.84	0.12
SD	3539	0.458	0.000	0.381	0.651	0.410	0.441	0.703	0.393	0.571	0.410	0.474	0.380	0.776	0.483	0.449	0.945	0.588	0.759			
RSD%	1.1	1.3	0.0	1.0	1.8	1.1	1.3	1.9	1.1	1.6	1.1	1.3	1.0	1.9	1.3	1.3	2.4	1.6	2.0			

(2 s.e.). Further information about the methodology are presented in Supplementary material.

3.2.3. LA-MC-ICP-MS

The Sm–Nd isotope measurements were carried out on a Thermo-Finnigan Neptune MC-ICP-MS, coupled with a 193 nm HelEx Photon-Machine laser ablation system, at the Laboratório de Geoquímica Isotópica (LOPAG), Universidade Federal de Ouro Preto. The experimental conditions and cup configurations for Nd isotopic analysis are given in Table 3.

The data reduction was performed using an offline Excel® spreadsheet by A. Gerdes (Frankfurt). Laser-induced elemental fractionation and instrumental mass discrimination were corrected and evaluated by two different approaches. The first round of analysis used NIST 610 as a primary reference material. A subsequent analytical session used the Namaqualand monazite (Liu et al., 2012) as a primary reference material and the results of both sessions were compared in order to evaluate the extent of matrix-effects for different reference materialization approaches. More information about the methodology and data reduction process are presented in Supplementary material.

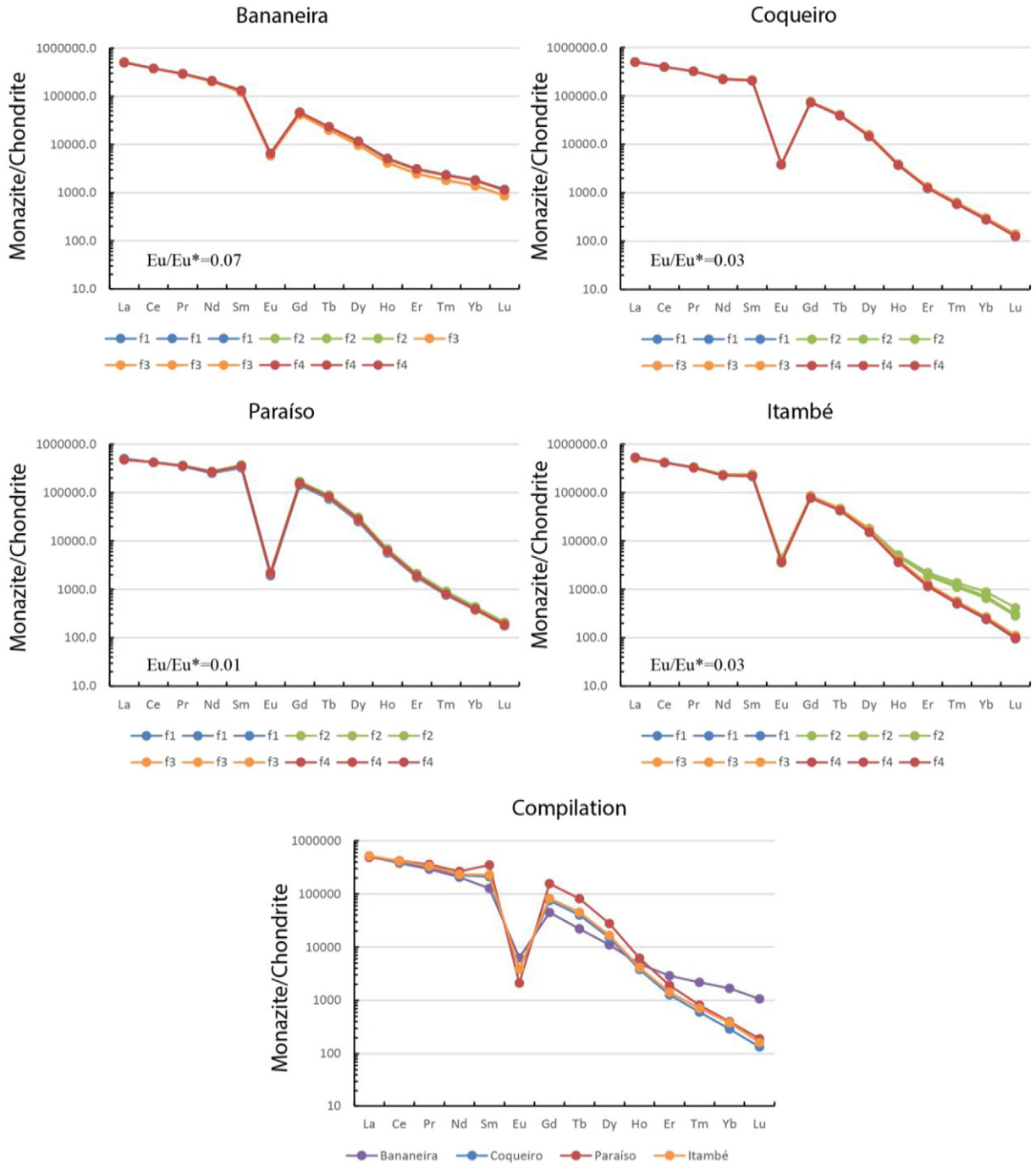

Fig. 5. Chondrite-normalized REE patterns of the monazites from this study. The compilations are the average results of three lines in four different fragments and the complete data are presented in Supplementary material. Concentrations were normalized by the chondrite values from Sun and McDonough (1989).

Table 6
LA-Q-ICP-MS average results for the studied monazites. The complete dataset can be found in Supplementary material. [a]Corrected for background and within-run Pb/U fractionation (in case of $^{206}Pb/^{238}U$); $^{207}Pb/^{235}U$ calculated using $^{207}Pb/^{206}Pb/(^{238}U/^{206}Pb^{*}1/137.88)$ [b]rho is the $^{206}Pb/^{238}U/^{207}Pb/^{235}U$ error correlation coefficient.

Sample	$^{206}Pb/^{238}U$[a]	±2σ (abs)	$^{207}Pb/^{235}U$[a]	±2σ (abs)	$^{208}Pb/^{232}Th$[a]	±2σ (abs)	$^{207}Pb/^{206}Pb$[a]	±2σ (abs)	rho[b]	$^{206}Pb/^{238}U$	±2σ (Ma)	$^{207}Pb/^{235}U$	±2σ (Ma)	$^{208}Pb/^{232}Th$	±2σ (Ma)	$^{207}Pb/^{206}Pb$	±2σ (Ma)
Bananeira (n = 49)	0.08140	0.00136	0.64166	0.01372	0.02464	0.00084	0.05717	0.00146	0.78	504	8	503	8	492	16	497	56
SD	0.00041	0.00002	0.00472	0.00046	0.00021	0.00002	0.00034	0.00004	0.02	2.4	0.1	2.9	0.3	4.1	0.3	13.3	1.4
RSD%	0.5	1.4	0.7	3.3	0.9	1.8	0.6	2.5	2.2	0.5	1.4	0.6	3.3	0.8	1.8	2.7	2.6
Coqueiro (n = 26)	0.08205	0.00135	0.65593	0.01748	0.02520	0.00085	0.05798	0.00186	0.63	508	8	512	11	503	17	529	70
SD	0.00070	0.00009	0.01069	0.00265	0.00036	0.00002	0.00082	0.00023	0.05	4.18	0.55	6.54	1.61	7.07	0.30	30.55	8.27
RSD%	0.9	6.9	1.6	15.1	1.4	2.0	1.4	12.1	7.6	0.8	6.8	1.3	15.1	1.4	1.8	5.8	11.8
Paraíso (n = 22)	0.08185	0.00129	0.64703	0.01575	0.02529	0.00085	0.05733	0.00172	0.65	507	8	507	10	505	17	504	66
SD	0.00069	0.00003	0.00799	0.00094	0.00031	0.00002	0.00040	0.00007	0.02	4.1	0.2	4.9	0.6	6.1	0.3	15.6	2.6
RSD%	0.8	2.6	1.2	6.0	1.2	1.8	0.7	4.3	3.2	0.8	2.6	1.0	5.8	1.2	1.5	3.1	4.0
Itambé (n = 56)	0.08176	0.00138	0.65080	0.01550	0.02488	0.00084	0.05776	0.00163	0.72	507	8	509	10	497	17	519	62
SD	0.00056	0.00007	0.00667	0.00270	0.00028	0.00003	0.00070	0.00026	0.09	3.4	0.4	4.1	1.7	5.5	0.6	18.7	10.0
RSD%	0.7	4.7	1.0	17.4	1.1	3.7	1.2	16.0	11.9	0.7	5.0	0.8	17.6	1.1	3.5	3.6	16.2
44069 (n = 127)	0.06826	0.00109	0.52085	0.01210	0.02124	0.00072	0.05534	0.00158	0.69	426	7	426	8	425	14	426	62
SD	0.00051	0.00006	0.00637	0.00116	0.00023	0.00002	0.00057	0.00014	0.06	3.1	0.3	4.3	0.8	4.6	0.4	22.8	5.1
RSD%	0.8	5.4	1.2	9.6	1.1	2.9	1.0	8.6	8.3	0.7	5.3	1.0	9.5	1.1	2.7	5.3	8.2

3.2.4. ID-TIMS

The monazite samples that yielded the most concordant populations from LA-Q-ICP-MS and LA-SF-ICP-MS dating were also dated by ID-TIMS (Isotope Dilution-Thermal Ionization Mass Spectrometry) in order to obtain high-precision "true ages" or "accepted values". Monazite ID-TIMS U–Pb geochronology were undertaken at the Jack Satterly Geochronology Laboratory (JSGL) at the University of Toronto (Canada) and in University of Oslo (Norway). At the JSG lab, the mass spectrometer used was a VG354 and in the Oslo lab a MAT262 was used. The methodologies used for each lab are found in Supplementary material.

4. Results

4.1. Chemical composition

The BSE images, presented in Fig. 3, shows that the monazite fragments from different samples were homogeneous in greyscale intensity (ie were compositionally homogeneous) and showed no evidence of mineral inclusions. Additional compositional maps performed by EDS are presented in the Supplementary material. The internal homogeneity was also evaluated through electron microprobe profiles along the different grains, each of them with approximately 500–200 μm long. For each grain, 12 points were made and the average results are shown in Table 4. The complete data set are presented in Supplementary material.

Itambé monazite, and samples from the three pegmatites, are similar in major element composition, and are compositionally uniform on a grain scale, consistent with the BSE images. Monazite from all samples have low CaO (0.44–0.93 wt%) and SiO_2 (0.94–0.1.64 wt%) concentrations. All can be classified as Ce-monazite, with monazite from Bananeira having the lowest Ce_2O_3 concentration (26.63 wt%). La_2O_3 concentrations are highest in Paraíso monazite (12.74 wt%), and lowest in Bananeira monazite (9.92 wt%), which has the highest Y contents (1.56 wt%).

The structural formula was calculated based on four oxygens following Pyle et al. (2001). The molar fractions of the monazite end-members of the system $2CePO_4$–$2ThSiO_4$–$CaTh(PO_4)_2$ (Bowie and Horne, 1953; Förster, 1998, Table 4) were calculated and were ploted in the ternary diagram of the Fig. 4A. All the samples can be classified as Ce-monazite ($2CePO_4$), with the samples having between 0.037–0.065 of the huttonite component ($ThSiO_4$). The brabantite component showed a similar behaviour, between 0.037–0.078 ($(Th,Ca,U,Pb)[PO4]_2$). The extent of brabantite vs huttonite exchange operational in monazite can be observed in a plot of Th + U + Si vs REE + Y + P (Fig. 4B). The huttonite exchange vector is clearly dominant in the samples, indicating that the $Ca^{2+} + Th^{4+} \leftrightarrow 2REE^{3+}$ (brabantite; Förster, 1998, Förster and Harlov, 1999), $Th^{4+} + Si^{4+} -> REE^{3+} + P^{5+}$ (huttonite; Della Ventura et al., 1996) and $U^{4+} + Si^{4+} \leftrightarrow REE^{3+} + P^{5+}$ (coffinite) coupled substitutions happened simultaneously.

The mineral compositions were also acquired using LA-Q-ICP-MS, performing three lines each on four different grain fragments. The chondrite normalized REE patterns (Table 5 and Fig. 5) are characterized by strong relative enrichment in LREEs, a clear relative depletion in HREEs and a large negative Eu anomaly (Eu/Eu^{*}; 0.07 for Bananeira, 0.03 for Coqueiro, 0.01 for Paraíso and 0.03 for Itambé monazite, respectively). The Paraíso monazite has a higher concentration of MREEs, with a slightly larger negative Eu anomaly, than the other monazite samples, whereas the Bananeira monazite is the most enriched in HREEs.

Based on the line traverses, the Coqueiro monazite is the most homogeneous in composition; monazites from Bananeira and Paraíso have slight compositional differences between grain fragments but within-grain fragment compositions are very uniform. Itambé monazite, however, shows differences between fragments, with one with significantly higher concentrations of the HREEs than the others. The Coqueiro, Paraíso and Itambé monazites show a strong fractionation of MREE/HREE ($(Gd/Lu)_N$ between 514 and 823) whereas the Bananeira sample has a small fractionation ($(Gd/Lu)_N = 42$) (Fig. 5).

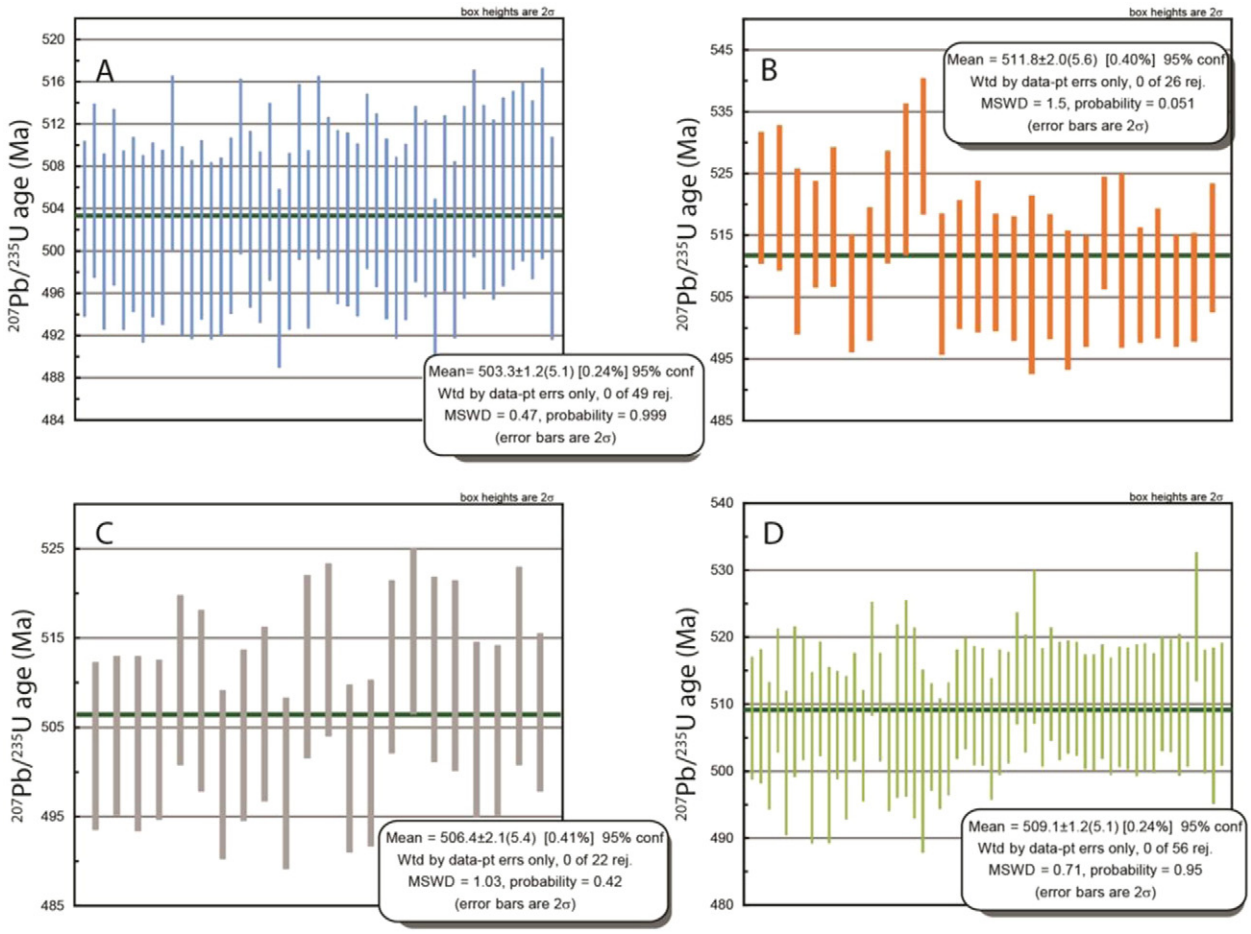

Fig. 6. Weighted average $^{207}Pb/^{235}U$ ages obtained by LA-Q-ICP-MS at UFOP. A-Bananeira, B-Coqueiro, C-Paraíso and D-Itambé monazites. The error quoted in parentheses is the realistic error (see text).

4.2. Isotopic characterization

4.2.1. LA-ICP-MS U–Pb geochronology

The LA-Q-ICP-MS (UFOP) analyses were performed in three different analytical sessions. For the Bananeira monazite (Table 6 and Fig. 6), 49 laser spot analyses yielded a weighted average $^{207}Pb/^{235}U$ age of 503.3 ± 5.1 Ma (95% confidence level or c.l.; MSWD = 0.47). It is important to highlight that, because of the high number of spots (to show homogeneity), the statistical errors on the average mean of all LA-ICP-MS analyses were typically lower than 0.1%. We therefore calculated a more realistic error based on the quadratic addition of the average mean error (given by Isoplot) and the 1% error inherent precision of the technique. This sample was also analysed at UFOP by LA-SF-ICP-MS (Table 7 and Fig. 7), with sixteen analysed laser spots yielding a weighted average $^{207}Pb^*/^{235}U$ age of 506.9 ± 6.1 Ma (95% c.l.; MSWD = 0.48).

Twenty-six analyses of the Coqueiro sample were undertaken by LA-Q-ICP-MS at UFOP (Table 6 and Fig. 6). These analyses yielded a weighted average $^{207}Pb/^{235}U$ age of 511.8 ± 5.6 Ma (95% c.l.; MSWD = 1.5). An additional seventeen laser spots were analysed using the LA-SF-ICP-MS (Table 7 and Fig. 7), resulting in a weighted average $^{207}Pb^*/^{235}U$ age of 510.4 ± 5.4 Ma (95% c.l.; MSWD = 0.99).

Paraíso sample had twenty two laser spot analyses by quadrupole (Table 7 and Fig. 7) and they yielded a weighted average $^{207}Pb/^{235}U$ age of 506.4 ± 5.4 Ma (95% c.l.; MSWD = 1.03). This sample has also been analysed by LA-SF-ICP-MS (Table 8 and Fig. 8), with the nineteen laser spot analyses yielding a weighted average $^{207}Pb^*/^{235}U$ age of 509.6 ± 5.4 Ma (95% c.l.; MSWD = 1.5).

The Itambé sample had fifty six laser spots analysed at UFOP by LA-Q-ICP-MS (Table 6 and Fig. 6) from four analytical sessions. All spots pooled together yielded a weighted average $^{207}Pb/^{235}U$ age of 509.1 ± 5.1 Ma (95% c.l.; MSWD = 0.71). The results are in agreement with a single LA-SF-ICP-MS (Table 7 and Fig. 7) session of thirty four laser spot analyses, which yielded a weighted average $^{207}Pb^*/^{235}U$ age of 504.6 ± 5.1 Ma (95% c.l.; MSWD = 0.71).

Monazite 44,069 (425 Ma; Aleinikoff et al., 2006) was used as the primary reference material for LA-ICP-MS geochronology at UFOP. One hundred and twenty seven analyses of this reference material on the LA-Q-ICP-MS (Table 6) yielded a weighted average $^{207}Pb/^{235}U$ age of 425.57 ± 4.3 Ma (95% c.l.; MSWD = 1.15), and thirty LA-SF-ICP-MS analyses yielded a weighted average $^{207}Pb^*/^{235}U$ age of 424.6 ± 4.4 Ma (95% c.l.; MSWD = 1.10; Table 7).

4.2.2. ID-TIMS U–Pb ages

U–Pb ID-TIMS analysis were carried out at the University of Toronto (Jack Satterly Geochronology Laboratory) and at the University of Oslo. We separated small fragments from the largest crystals (one Itambé and one Bananeira). The random fragments that were analysed are from the exact same crystal that the LA-ICP-MS data were acquired. Itambé monazite was selected because it is the fragment of the original Moacyr monazite and the Bananeira because it gave the most consistent LA-ICP-MS U–Pb results, ie, showed the lowest values of RSD% for a given age or ratio (see previous section). The shards were aproximally 200 μm long.

Table 7
LA-SF-ICP-MS average results for the studied monazites. The complete dataset can be found in Supplementary material. The error of the ages is the quadratic additions of the within run precision (2SE) and the external reproducibility (2SD) of the reference monazite. $^{207}Pb/^{206}Pb$ error propagation (^{207}Pb signal dependent) following Gerdes and Zeh (2009). $^{207}Pb/^{235}U$ error is the quadratic addition of the $^{207}Pb/^{206}Pb$ and $^{206}Pb/^{238}U$ uncertainty. [a]Within run background-corrected mean ^{207}Pb signal in cps (counts per second); [b]corrected for background, within-run Pb/U fractionation (in case of $^{206}Pb/^{238}U$) and common Pb using Stacey and Kramers (1975) model for Pb composition and subsequently normalized to reference monazite (ID-TIMS value/measured value): $^{207}Pb/^{235}U$ calculated using $^{207}Pb/^{206}Pb$ ($^{238}U/^{206}Pb * 1/137.88$); [c]rho is the $^{206}Pb/^{238}U$-$^{207}Pb/^{235}U$ error correlation coefficient.

Sample	^{207}Pb [a] (cps)	$^{206}Pb/^{204}Pb$	$^{206}Pb/^{238}U$ [b]	±2σ (abs)	$^{207}Pb/^{235}U$ [b]	±2σ (abs)	$^{208}Pb/^{232}Th$ [b]	±2σ (abs)	$^{207}Pb/^{206}Pb$ [b]	±2σ (abs)	rho[c]	$^{206}Pb/^{238}U$	±2σ (Ma)	$^{207}Pb/^{235}U$	±2σ (Ma)	$^{208}Pb/^{232}Th$	±2σ (Ma)	$^{207}Pb/^{206}Pb$	±2σ (Ma)
Bananeira (n = 16)	1835	9610	0.08129	0.00179	0.64815	0.02368	0.01447	0.00024	0.05783	0.00222	0.61	504	11	507	15	290	5	523	84
SD	76	13470	0.00048	0.00009	0.00760	0.00324	0.00074	0.00002	0.00056	0.00030	0.05	2.9	0.5	4.7	2.0	14.7	0.3	21.3	11
RSD%	4.1	140.2	0.6	4.8	1.2	13.7	5.1	7.7	1.0	13.6	8.2	0.6	4.7	0.9	13.5	5.1	7.2	4.1	13.1
Coqueiro (n = 17)	7807	18916	0.08183	0.00130	0.65340	0.01354	0.02603	0.00024	0.05791	0.00144	0.77	507	8	511	8	519	5	526	54
SD	416	40842	0.00047	0.00002	0.00689	0.00103	0.00027	0.00001	0.00054	0.00009	0.05	2.8	0.1	4.2	0.6	5.3	0.2	20.4	3
RSD%	5.3	215.9	0.6	1.5	1.1	7.6	1.0	4.6	0.9	6.1	5.9	0.6	1.4	0.8	7.5	1.0	4.3	3.9	5.6
Paraíso (n = 19)	4179	17477	0.08226	0.00125	0.65183	0.01349	0.02535	0.00086	0.05747	0.00003	0.73	510	6	510	7	506	17	510	28
SD	2489	38748	0.00073	0.00016	0.00693	0.00142	0.00028	0.00001	0.00022	0.00000	0.05	4.3	0.0	4.3	0.0	5.6	0.2	8.5	0
RSD%	59.6	2.2	0.9	0.1	0.0	0.1	0.0	0.0	0.0	0.0	0.1	0.0	0.0	0.0	0.0	0.0	0.0	0.0	0.0
Itambé (n = 34)	11767	67569	0.08170	0.00119	0.64377	0.01132	0.02507	0.00016	0.05715	0.00130	0.83	506	7	505	7	500	3	497	50
SD	657	92484	0.00044	0.00002	0.00479	0.00063	0.00033	0.00001	0.00039	0.00005	0.03	2.6	0.1	3.0	0.4	6.4	0.1	15.1	2
RSD%	5.6	136.9	0.5	2.0	0.7	5.6	1.3	5.2	0.7	3.8	4.0	0.5	1.8	0.6	5.5	1.3	3.8	3.0	3.4
44069 (n = 30)	6678	33467	0.06811	0.00114	0.51933	0.01228	0.02127	0.00021	0.05530	0.00153	0.75	425	7	425	8	425	4	424	61
SD	3739	57803	0.00055	0.00022	0.00563	0.00475	0.00081	0.00010	0.00051	0.00045	0.10	3.3	1.3	3.8	3.2	16.0	1.9	20.5	17
RSD%	56.0	172.7	0.8	19.3	1.1	38.6	3.8	45.0	0.9	29.3	13.3	0.8	19.3	0.9	38.7	3.8	44.8	4.8	28.8

For the Itambé monazite (Table 8 and Fig. 8), one of the eight points was discarded due to discordance. If we disregard this analysis, the seven monazite fractions yielded weighted average $^{207}Pb^*/^{235}U$, $^{206}Pb^*/^{238}U$ and $^{207}Pb^*/^{206}Pb^*$ ratios of 0.6467 ± 0.0012 (95% c.l.; MSWD = 1.5), 0.082628 ± 0.000087 (95% c.l.; MSWD = 0.93) and 0.056750 ± 0.000024 (one point rejected; 95% c.l.; MSWD = 1.16), respectively. The corresponding $^{207}Pb^*/^{235}U$, $^{206}Pb^*/^{238}U$ and $^{207}Pb^*/^{206}Pb^*$ weighted average ages are 506.44 ± 0.73 Ma (95% c.l.; MSWD = 1.5), 511.79 ± 0.52 Ma (95% c.l.; MSWD = 0.93) and 481.82 ± 0.91 Ma (95% c.l.; MSWD = 1.17). The best estimate of the crystallization age of the monazite is the $^{207}Pb^*/^{235}U$ age (506.44 ± 0.73 Ma), and is in agreement, within error, with the LA-ICP-MS data. Which is very similar to some of TIMS ages obtained from "Moacyr/Moacir" monazite e.g. the unpublished TIMS ages quoted in Kohn and Vervoort (2008), Dumond et al. (2008) and published ages of Gasquet et al. (2010; Fig. 9).

U–Pb ID-TIMS data obtained for the Bananeira sample also had one of the eight points discarded due to discordance (Table 8 and Fig. 8). The weighted mean $^{207}Pb^*/^{235}U$, $^{206}Pb^*/^{238}U$ and $^{207}Pb^*/^{206}Pb^*$ ratios obtained by the remaining seven aliquots are 0.6487 ± 0.0021 (95% c.l.; MSWD = 6.8), 0.08294 ± 0.00021 (95% c.l.; MSWD = 6.6) and 0.056723 ± 0.000051 (95% c.l.; MSWD = 2.4), respectively; yielding weighted mean ages of 507.7 ± 1.3 Ma (95% c.l.; MSWD = 6.8), 513.6 ± 1.2 Ma (95% c.l.; MSWD = 6.6), and 480.8 ± 2.0 Ma (95% c.l.; MSWD = 2.4), respectively. The weighted mean $^{207}Pb^*/^{235}U$ age of 507.7 ± 1.3 Ma provides the best estimate of the crystallization age of this monazite, and is equivalent within error to the data obtained from the Itambé monazite sample and to the LA-ICP-MS data. This age is also very similar to some of TIMS ages obtained to "Moacyr/Moacir" in the literature (see above).

4.2.3. Sm–Nd isotope composition

The first set of analyses was performed using NIST 610 as a primary reference material. All the results are quoted as the average of the values and errors as reference material deviation (2SD) of the same values. The mounts analysed are the same that were used in the previous sections. The fragments were between 200 and 500 μm long.

The Bananeira sample had 65 points analysed in six different shards obtained from one bigger crystal (Table 9). This sample showed a somewhat heterogeneous radiogenic Sm–Nd isotopic composition; individual fragments were internally homogeneous on a length scale of 4 mm, but differed in $^{147}Sm/^{144}Nd$ from other fragments. The mean $^{147}Sm/^{144}Nd$ values from individual fragments varied from 0.2742 ± 6 (2SD) to 0.2839 ± 4 (2SD) with an overall value for the six fragments of 0.2775 ± 74 (2SD). In contrast, the $^{143}Nd/^{144}Nd$ mean values from the different fragments varied from 0.512748 ± 27 (2SD) to 0.512784 ± 23 (2SD), yielding a general mean value of 0.512763 ± 38 (2SD), a much smaller variation. The εNdi values of the fragments ranged from −2.3 ± 0.4 (2SD) to −3.4 ± 0.4 (2SD) and yielded an average value of −2.8 ± 0.2 (SD). The mean $^{145}Nd/^{144}Nd$ value of 0.34841 ± 1 (2SD) is in agreement with the recommended value of 0.348415 (Wasserburg et al., 1981). On a plot of $^{147}Sm/^{144}Nd$ v. $^{143}Nd/^{144}Nd$ the data do not plot together, forming three different groups of values, but are consistent with the 508 Ma (ID-TIMS $^{207}Pb/^{235}U$ age for this sample) reference isochron (Fig. 9). The relative reference material deviation (RSD%) for the $^{147}Sm/^{144}Nd$ ratio is 2.66% and 0.007% for the $^{143}Nd/^{144}Nd$ ratio. The variation in $^{147}Sm/^{144}Nd$, in particular, is bigger in comparison to proposed Sm–Nd reference monazites such as Namaqualand and Managountry (Liu et al., 2012; Fig. 10).

The Coqueiro monazite had 86 points analysed from six different fragments (Table 9). This sample also showed a somewhat heterogeneous radiogenic Sm–Nd isotopic composition, although $^{147}Sm/^{144}Nd$ ratios were again homogeneous within individual grain fragments. The mean $^{147}Sm/^{144}Nd$ values ranged from 0.2016 ± 5 (2SD) to 0.2129 ± 4 (2SD) yielding an overall average value of 0.2073 ± 64 (2SD). The $^{143}Nd/^{144}Nd$ ratio ranged from 0.512487 ± 27 (2SD) to

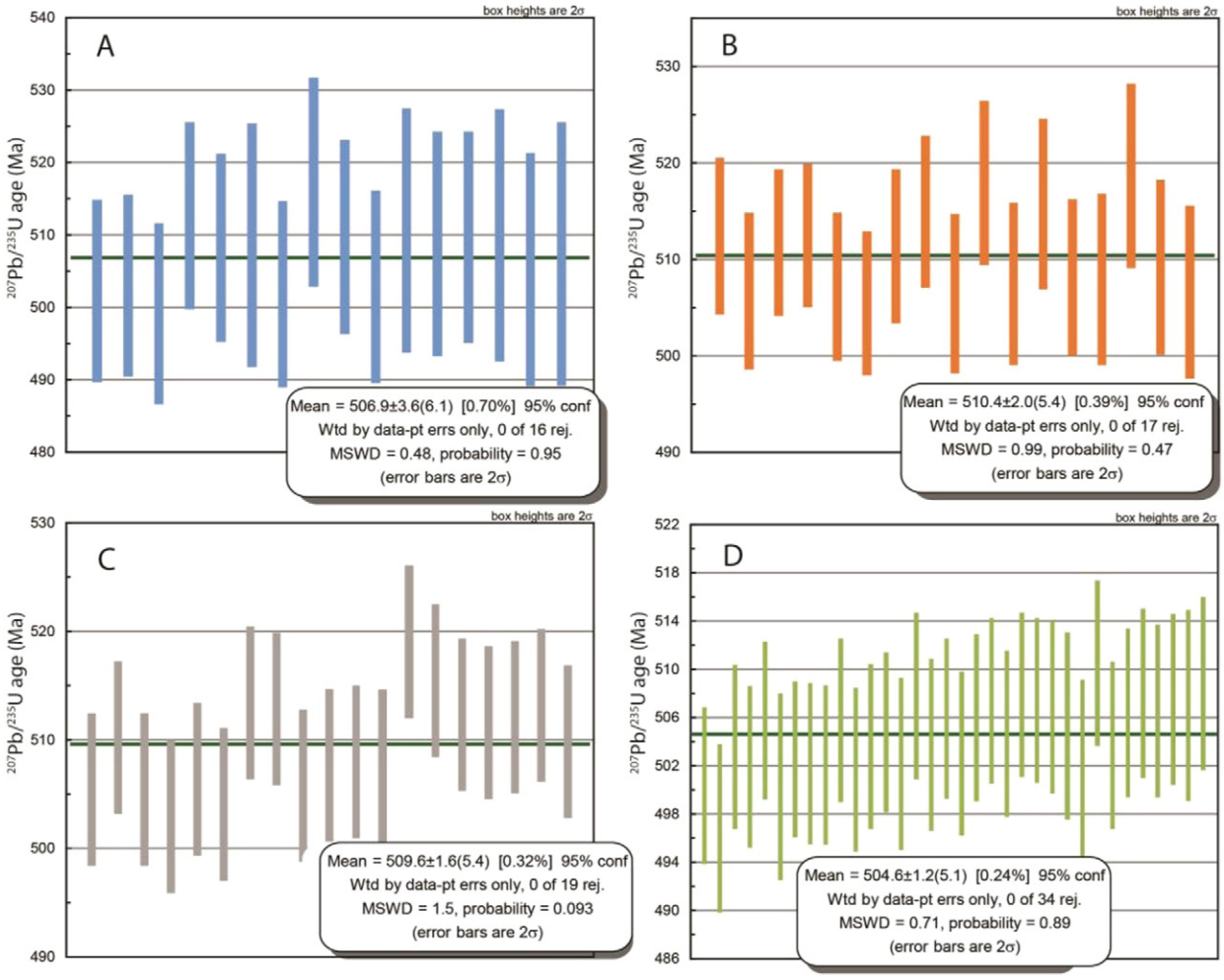

Fig. 7. Weighted average $^{207}Pb/^{235}U$ ages obtained by LA-SF-ICP-MS at UFOP. A-Bananeira, B-Coqueiro, C-Paraíso and D-Itambé monazites. The error quoted in parentheses is the realistic error (see text).

0.512510 ± 26 (2SD), yielding an overall value of 0.512497 ± 27 (2SD). The εNdi value of the different crystal shards ranged between −3.2 ± 0.2 (SD) to −3.6 ± 0.3 (SD), yielding an average value of −3.4 ± 0.3 (SD). The mean $^{145}Nd/^{144}Nd$ value of 0.34841 ± 1 (2SD) was also in agreement with the recommended value of Wasserburg et al. (1981). As with the Bananeira sample, a plot of $^{147}Sm/^{144}Nd$ versus $^{143}Nd/^{144}Nd$ shows that the data do not group together, but instead form three clusters that are consistent with the 510 Ma ($^{207}Pb/^{235}U$ LA-ICP-MS age for this sample) reference isochron (Fig. 9). The RSD% for the $^{147}Sm/^{144}Nd$ ratio is 3.10% and 0.005% for the $^{143}Nd/^{144}Nd$. These variations, particularly for the $^{147}Sm/^{144}Nd$ ratio, are larger than those for the Namaqualand and Managountry monazites (Liu et al., 2012; Fig. 10).

The Paraíso sample had 75 points analysed in three different crystal fragments (Table 9). One of the three chips showed a different $^{147}Sm/^{144}Nd$ isotopic composition than the other homogeneous two. The $^{147}Sm/^{144}Nd$ mean values ranged from 0.2761 ± 2 (2SD) to 0.2857 ± 4 (2SD), with a general value of 0.2833 ± 73 (2SD). The $^{143}Nd/^{144}Nd$ values ranged from 0.512761 ± 24 (2SD) to 0.512791 ± 15 (2SD) and yielded an overall average value of 0.512784 ± 29 (2SD). Even though there were small variations in the isotopic ratios, the εNdi of the fragments agrees within error to one another with an average value −2.8 ± 0.2 (SD). The $^{145}Nd/^{144}Nd$ average value is 0.34841 ± 1 (2SD), compatible to the canonical value from Wasserburg et al. (1981). The plot of $^{147}Sm/^{144}Nd$ versus $^{143}Nd/^{144}Nd$ shows that the data do not group together, forming three different groups of values, consistent with the 510 Ma (U–Pb LA-ICP-MS Concordia age for this sample) reference isochron (Fig. 9). The RSD% for the $^{147}Sm/^{144}Sm$ ratio is 2.59% and 0.006% for the $^{143}Nd/^{144}Nd$. Those variations are also bigger in comparison to the Namaqualand and Managountry monazites (Liu et al., 2012) but very similar to the variations of the Bananeira sample (Fig. 10).

The Itambé monazite had 49 analysed points in two large fragments (Table 9). The two fragments have slightly different $^{147}Sm/^{144}Nd$ isotopic compositions. The $^{147}Sm/^{144}Nd$ values ranged from 0.1938 ± 2 (2SD) to 0.1980 ± 9 (2SD), yielding an overall value of 0.1955 ± 41 (2SD). The $^{143}Nd/^{144}Nd$ values are relatively homogeneous resulting in an average of 0.512424 ± 24 (2SD). Those narrow variations on the $^{147}Sm/^{144}Nd$ ratios did not change the εNdi value, yielding an average value of −4.1 ± 0.2 (SD). The mean $^{145}Nd/^{144}Nd$ value is 0.34840 ± 1 (2SD), which is within error of the recommended value of Wasserburg et al. (1981). The plot $^{147}Sm/^{144}Nd$ versus $^{143}Nd/^{144}Nd$ shows that again the data do not group together, forming two different groups of values but are consistent with the 506 Ma (ID-TIMS $^{207}Pb/^{235}U$ age for this sample) reference isochron (Fig. 9). Furthermore, the RSD% for the $^{147}Sm/^{144}Sm$ ratio is 2.12% and 0.005% for the $^{143}Nd/^{144}Nd$ ratio. The variations of the $^{147}Sm/^{144}Nd$ ratio are similar to proposed reference material Managountry monazite but bigger than the Namaqualand reference material monazite (Liu et al., 2012; Fig. 10). Comparing the RSD% of this sample to the other monazites from the Itambé district, the Itambé monazite is the most homogeneous sample (Fig. 10).

In order to evaluate a possible matrix effect due to normalization to the NIST 610 glass, another analytical session were performed using,

Table 8
ID-TIMS U–Pb results. (a) Th/U calculated from radiogenic $^{208}Pb/^{206}Pb$ ratio and $^{207}Pb/^{206}Pb$ age assuming concordance; (b) PbC is total amount of common Pb in picograms; 1 pg Pb assigned the isotopic composition of laboratory blank; initial Pb corrected using Pb evolution model of Stacey and Kramers (1975); (c) measured $^{206}Pb/^{204}Pb$ corrected for fractionation and spike; (d) corrected for fractionation, spike, blank and initial Pb; (e) rho is correlation coefficients of X–Y errors on the Concordia plot; (f) Disc is percent discordance for the given $^{207}Pb/^{206}Pb$ age; (g) corrected for fractionation, spike and blank only; *Oslo University, **Toronto University. The analyses in italic were not used in the age calculations.

Sample	Weight [μg]	U [ppm]	Th/U (a)	PbC [pg] (b)	$^{206}Pb/^{204}Pb$ measured (c)	Corrected for fractionation, spike, blank and initial common Pb: $^{207}Pb/^{235}U$ (c)	$\pm 2\sigma$ [abs]	$^{206}Pb/^{238}U$ (c)	$\pm 2\sigma$ [abs]	rho (e)	$^{207}Pb/^{206}Pb$ (c)	$\pm 2\sigma$ [abs]	$^{207}Pb/^{235}U$ [Ma] (c)
Itambé**	21	57963	27.4	1101	5746	0.6518	0.0041	0.08301	0.00050	0.93	0.05695	0.00013	509.6
Itambé**	7	141907	28.3	1287	3996	0.6477	0.0029	0.08261	0.00030	0.78	0.05687	0.00016	507.1
*Itambé***	*35*	*183201*	*28.6*	*235*	*8211*	*0.3738*	*0.0153*	*0.04814*	*0.00196*	*0.99*	*0.05632*	*0.00027*	*322*
Itambé*	9	>2100	28.1	16.1	6071	0.6449	0.0031	0.08234	0.00036	0.95	0.05680	0.00008	505.3
Itambé*	1	>4500	26.4	5.5	4264	0.6465	0.0031	0.08256	0.00037	0.96	0.05679	0.00008	506.3
Itambé*	50	>830	25.9	28.6	7578	0.6466	0.0016	0.08265	0.00019	0.96	0.05674	0.00004	506.4
Itambé*	66	>570	27.1	27.4	7150	0.6461	0.0015	0.08260	0.00017	0.94	0.05673	0.00005	506.1
Itambé*	12	>1820	26.6	18.6	6117	0.6468	0.0016	0.08268	0.00018	0.94	0.05674	0.00005	506.5
Bananeira*	3	>3900	27.5	16.2	3763	0.6462	0.0017	0.08274	0.00017	0.90	0.05665	0.00006	506.1
Bananeira*	8	>1300	27.0	14.0	3863	0.6464	0.0017	0.08273	0.00017	0.89	0.05667	0.00007	506.3
Bananeira*	2	>4700	27.3	12.9	3806	0.6469	0.0018	0.08271	0.00017	0.84	0.05673	0.00009	506.6
Bananeira*	1	>2700	27.3	6.1	2306	0.6507	0.0021	0.08313	0.00018	0.76	0.05677	0.00012	508.9
Bananeira*	57	>1600	28.6	108.0	4384	0.6518	0.0017	0.08330	0.00018	0.92	0.05676	0.00006	509.6
Bananeira*	2	>2300	28.6	5.6	4337	0.6493	0.0016	0.08298	0.00017	0.89	0.05675	0.00006	508.0
Bananeira*	2	>1800	27.1	4.6	4181	0.6502	0.0018	0.08302	0.00017	0.86	0.05680	0.00008	508.6
*Bananeira**	*1*	*>1600*	*29.9*	*8.5*	*817*	*0.5452*	*0.0033*	*0.06976*	*0.00025*	*0.69*	*0.05668*	*0.00025*	*441.8*

Sample	Corrected for fractionation, spike, blank and initial common Pb:						Corrected for fractionation, spike and blank:						
	±2σ [abs]	$^{206}Pb/^{238}U$ [Ma] (c)	±2σ [abs]	$^{207}Pb/^{206}Pb$ [Ma] (c)	±2σ [abs]	Disc [%] (f)	$^{206}Pb/^{204}Pb$ (g)	$^{207}Pb/^{204}Pb$ (g)	$^{208}Pb/^{204}Pb$ (g)	$^{206}Pb/^{238}U$ (g)	±2σ [abs]	$^{207}Pb/^{206}Pb$ (g)	±2σ [abs]
Itambé**	2.5	514.1	3.0	489	5	−5.2	5797	345	49217	12.010	0.073	0.05945768	0.000078
Itambé**	1.8	511.7	1.8	486	6	−5.4	4026	244	35285	12.052	0.043	0.06048259	0.000048
*Itambé***	*11*	*303*	*12*	*465*	*11*	*36*	*8564*	*497*	*76193*	*20.731*	*0.863*	*0.05802208*	*0.00027938*
Itambé*	1.9	510.1	2.1	483.9	3.3	−5.6	6937	409	62411	12.113	0.052	0.0589018	0.00007
Itambé*	1.9	511.4	2.2	483.4	3.1	−6.0	6682	394	56512	12.080	0.052	0.0589704	0.00007
Itambé*	1.0	511.9	1.1	481.5	1.7	−6.6	8150	477	67517	12.073	0.027	0.0585298	0.00004
Itambé*	1.0	511.6	1.0	481.0	1.8	−6.6	7716	452	66976	12.078	0.024	0.058617	0.00005
Itambé*	1.0	512.1	1.0	481.4	1.9	−6.6	6859	404	58296	12.063	0.025	0.0588621	0.00004
Bananeira*	1.0	512.4	1.0	477.8	2.5	−7.5	4293	258	37672	12.036	0.024	0.060041	0.000054
Bananeira*	1.1	512.4	1.0	478.6	2.6	−7.4	4508	270	38931	12.039	0.024	0.05989756	0.000061
Bananeira*	1.1	512.3	1.0	480.9	3.4	−6.8	4506	270	39267	12.042	0.024	0.05995971	0.000083
Bananeira*	1.3	514.8	1.1	482.7	4.6	−6.9	3438	210	30024	11.966	0.026	0.0610083	0.0001
Bananeira*	1.0	515.8	1.1	482.1	2.2	−7.3	4467	268	40855	11.957	0.026	0.0600178	0.00004
Bananeira*	1.0	513.9	1.0	481.7	2.5	−7.0	6738	397	61558	12.019	0.024	0.0589085	0.00005
Bananeira*	1.1	514.1	1.0	483.6	3.1	−6.6	7420	436	64399	12.016	0.025	0.0587586	0.00007
*Bananeira**	*2.2*	*434.7*	*1.5*	*479.0*	*9.8*	*9.5*	*1064*	*75*	*9219*	*14.092*	*0.061*	*0.0703744*	*0.00015*

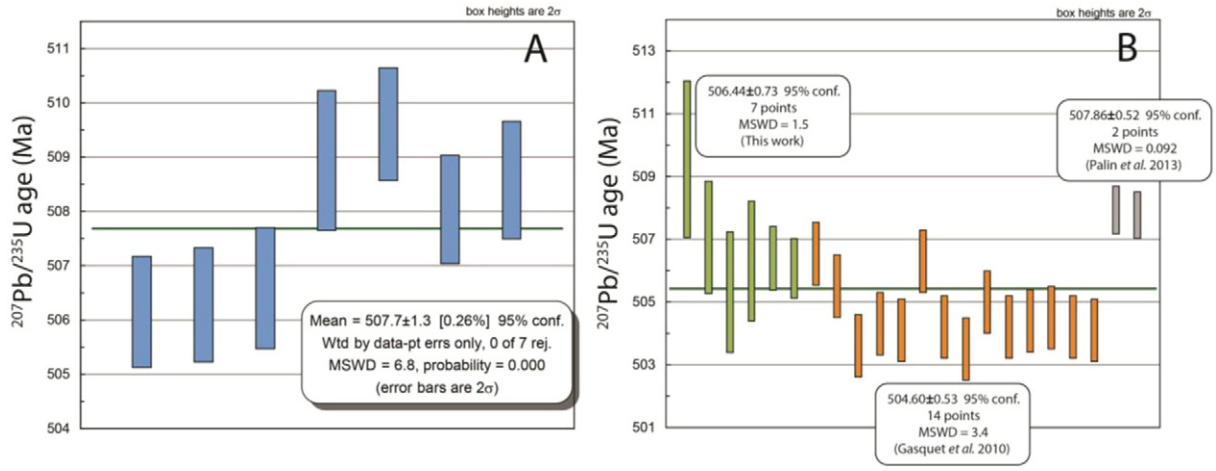

Fig. 8. ID-TIMS U–Pb weighted mean age $^{207}Pb^*/^{235}U$ results for Bananeira (A) and Itambé (B), for this last ID-TIMS data for Gasquet et al. (2010) (orange) and Palin et al. (2013) (grey) are also included for comparison with the data obtained by this work (green).

instead of the synthetic glass, the Namaqualand (Steenkampskral) monazite reference material (Liu et al., 2012; Table 10). In this session, only Itambé monazite sample was analysed. The 39 points obtained from two fragments, in general, showed the same behaviour regardless of the reference material used. In contrast to the data generated using the NIST glass as a reference material, the $^{147}Sm/^{144}Nd$ values were within error of each other, yielding an average value of 0.2000 ± 30 (2SD). The $^{143}Nd/^{144}Nd$ values were homogeneous in 0.512463 ± 30 (2SD). The εNdi value average was slight lower than the obtained by normalization to synthetic glass but, within error, did not change, yielding an average value of −3.6 ± 0.3 (SD). The weighted average $^{145}Nd/^{144}Nd$ value is 0.34841 ± 2 (2SD), again in agreement with the recommended value of Wasserburg et al. (1981).

Because of the small spread in Sm/Nd ratios (e.g., Fig. 9), it was also important to evaluate possible effects of downhole fractionation on the Nd/Nd and Sm/Nd ratios. Fig. 12 shows a time-resolved pattern (i.e., down-hole) of one analysis of the Itambé monazite. The variations measured in the $^{147}Sm/^{144}Nd$ ratio through time do not form a descendant line that is characteristic of the down-hole fractionation but rather a very narrow compositional variation in the order of ±0.001 (Fig. 11). This variation is one order of magnitude smaller (±0.01) than the variations observed in Fig. 10 for the same point or between fragments. Furthermore, the variations are observed in the time-resolved pattern of the $^{143}Nd/^{144}Nd$ ratio (0.00001; Fig. 11), are also smaller then the variations observed in the samples (Fig. 9), and therefore no possible effect of downhole fractionation was detected.

5. Discussion

In order to have a monazite to be used as a U–Pb reference material for LA-ICP-MS, it should fulfil some requirements, similar to the proposed by Sláma et al. (2008) for zircon: (i) homogeneity and concordance of radiogenic Pb/U ratios; (ii) low common Pb content; (iii) moderate U content (tens to hundreds ppm); (iv) crystalline (nonmetamict) structure; (v) size suitable for repeated laser ablation analyses (grains several mm to cm in diameter) and (vi) availability to the scientific community. In the case of a Sm–Nd monazite reference material, Iizuka et al. (2011) and Liu et al. (2012) suggest that the reference material must fulfil the following criteria: (i) matrix matching; (ii) it must have had an initially homogeneous Nd isotopic composition; (iii) its Sm–Nd isotope system must remain undisturbed and (iv) it must be available in large quantities of coarse-grained, gem-quality crystals, for distribution among different LA-ICP-MS laboratories.

In either case, the internal homogeneity is a crucial parameter for any potential reference material. This homogeneity is important because the mean values of the monazite must be representative for any small chip or fragment that is included in a LA-ICP-MS mount.

5.1. U–Pb reference material evaluation

According to the BSE images and compositional maps, all the samples are internally homogeneous, an important characteristic of a good LA-ICP-MS natural reference material (e.g. Sláma et al., 2008, Nasdala et al., 2008). The electron microprobe analysis characterized the monazites as monazite-(Ce), with negligible amount of the huttonite and brabantite component (Table 4 and Fig. 4).

The U–Pb results of the different monazites analysed in this study are summarized in Tables 6, 7 and 8. Monazite distributed under the name Moacyr/Moacir has also been used as a U–Pb reference material for a number of studies using LA-ICP-MS (e.g. Paquette and Tiepolo, 2007; Kohn and Vervoort, 2008; Dumond et al., 2008; Gasquet et al., 2010) or SIMS (Harley and Nandakumar, 2014) approaches. A piece of this monazite termed Itambé has been recently characterized as a reference material for oxygen isotope analysis by SIMS (Rubatto et al., 2014). However, the exact locality (or localities) from which the different pieces of Moacyr/Moacir monazite were obtained is unclear (see discussion below).

The Itambé monazite crystal is characterized by hight contents of U (up to 183,201 ppm) and narrow Th/U (25.9–28.6; Table 8) variations. The ID-TIMS results shows relatively high contents of initial common lead and reverse discordance. One of the eight splits was significantly discordant and was therefore not included in the mean calculations. As the U content is extremely high, the common Pb contents did not greatly affect the ages. Reverse discordance in TIMS analyses of monazite is partly attributed to "excess" ^{206}Pb from the decay of ^{230}Th (e.g., Harrison et al., 2002; Kohn and Vervoort, 2008; Fletcher et al., 2012). This can also be seen as the high Th content in the Itambé is responsible for the slight disequilibrium of the $^{206}Pb/^{238}U$ system (Gasquet et al., 2010). Also a disequilibrium in the U–Pb–Th system cannot be discarded. Considering that the $^{207}Pb/^{235}U$ ratio remains almost undisturbed by radioactive disequilibria in the U series (Schärer, 1984), here we consider the age for this ratio as the crystallization time for our samples. The results of LA-Q-ICP-MS and LA-SF-ICP-MS show good agreement with

Table 9
Sm–Nd isotopic compositions of the monazite samples determined by LA-MC-ICP-MS from this study using NIST610 as reference material. Each grain is the average result of at least ten points divided in different grains. [a]Number of points on each grain; [b]ratio corrected for inter-element fractionation using NIST610; [c]mass bias correction using exponential law; [d]all ratios are corrected for mass fractionation using exponential law; [e]initial ratio corrected regarding U–Pb age; [f]reference age obtained by ID-TIMS or LA-ICP-MS (see on text).

Sample	Grain	Nd_{tot} (V)	$^{147}Sm/^{144}Nd$	±2σ	βSm[c]	βNd[c]	$^{145}Nd/^{144}Nd$	$^{148}Nd/^{144}Nd$	$^{150}Nd/^{144}Nd$	$^{143}Nd/^{144}Nd$	±2σ	$^{143}Nd/^{144}Nd_i$	eNd_i	±2σ	Age
Bananeira	1 (n = 4)	56.2	0.2839	0.0006	−1.51	−1.71	0.348409	0.241527	0.214798	0.512784	0.000011	0.511841	−2.8	0.4	508
	2 (n = 8)	52.8	0.2811	0.0006	−1.50	−1.70	0.348410	0.241534	0.226840	0.512782	0.000010	0.511849	−2.7	0.4	
	3 (n = 7)	51.0	0.2814	0.0006	−1.50	−1.70	0.348410	0.241531	0.232001	0.512782	0.000011	0.511847	−2.7	0.4	
	4 (n = 9)	49.6	0.2813	0.0006	−1.50	−1.70	0.348410	0.241532	0.232319	0.512776	0.000011	0.511846	−2.8	0.4	
	5 (n = 20)	44.2	0.2746	0.0006	−1.51	−1.71	0.348410	0.241535	0.236618	0.512751	0.000011	0.511845	−2.8	0.4	
	6 (n = 18)	43.4	0.2742	0.0006	−1.52	−1.72	0.348408	0.241538	0.237112	0.512748	0.000012	0.511838	−2.9	0.4	
Coqueiro	1 (n = 15)	49.7	0.2067	0.0004	−1.50	−1.70	0.348414	0.241543	0.236753	0.512505	0.000010	0.511818	−3.3	0.4	510
	2 (n = 15)	48.5	0.2016	0.0005	−1.52	−1.72	0.348414	0.241540	0.238270	0.512491	0.000012	0.511821	−3.2	0.4	
	3 (n = 15)	49.6	0.2069	0.0004	−1.54	−1.74	0.348412	0.241547	0.236162	0.512493	0.000010	0.511806	−3.5	0.4	
	4 (n = 15)	50.1	0.2077	0.0004	−1.54	−1.74	0.348414	0.241549	0.235932	0.512496	0.000010	0.511806	−3.5	0.4	
	5 (n = 15)	49.2	0.2129	0.0004	−1.55	−1.75	0.348412	0.241551	0.236060	0.512510	0.000011	0.511803	−3.6	0.4	
	6 (n = 15)	50.0	0.2071	0.0004	−1.56	−1.76	0.348410	0.241555	0.235626	0.512487	0.000010	0.511799	−3.6	0.4	
Paraíso	1 (n = 30)	52.0	0.2845	0.0003	−1.50	−1.70	0.348413	0.241526	0.229563	0.512788	0.000010	0.511843	−2.8	0.4	510
	2 (n = 30)	50.2	0.2857	0.0003	−1.52	−1.72	0.348413	0.241530	0.233245	0.512791	0.000010	0.511842	−2.8	0.4	
	3 (n = 15)	48.6	0.2761	0.0003	−1.53	−1.73	0.348410	0.241533	0.234889	0.512761	0.000010	0.511844	−2.8	0.4	
Itambé	1 (n = 29)	45.6	0.1938	0.0004	1.58	−1.78	0.348403	0.241563	0.237369	0.512421	0.000011	0.511777	−4.1	0.4	506
	2 (n = 20)	48.4	0.1980	0.0004	1.59	−1.79	0.348400	0.241569	0.237026	0.512428	0.000011	0.511770	−4.2	0.4	

the obtained values of the ID-TIMS from this study. The values for the ID-TIMS of 506.44 ± 0.73 Ma for the $^{207}Pb^*/^{235}U$ age agrees, within error, with previously published ages of 504 ± 0.2 Ma (Gasquet et al., 2010), 506 ± 1 Ma (Dumond et al., 2008) and 507.86 ± 0.52 (Palin et al., 2013; Fig. 9).

The Bananeira monazite has been previously dated at 520 Ma by EPMA (Cruz et al., 1966) and in 508.9 ± 0.9 (0.18% 2SE, MSWD = 1.9) for the $^{206}Pb/^{238}U$ and a $^{208}Pb/^{232}Th$ age of 497.6 ± 1.6 (0.32% 2SE, MSWD = 6.1; Kylander-Clark et al., 2013). Fletcher et al. (2012) have considered the monazite from the Bananeira pegmatite as the "Moacyr" and thus compared its results with different works that used it as reference material (e.g. Seydoux-Guillaume et al., 2002; Gasquet et al., 2010). On the other hand, they did not provide tables in order to compare the data and correlate it the other monazites from the Itambé district. This sample was also used as reference material in several studies, such as Goudie et al. (2014, U–Pb secondary reference material) and in Kylander-Clark et al. (2013) for a REE reference material.

The U–Pb ID-TIMS data for the Bananeira monazite in this study are similar to those of the Itambé sample. Bananeira monazite is characterized by a relatively lower contents of U (<4700 ppm) and narrow Th/U variations (27.01–27.45; Table 8). The ID-TIMS data also shows relatively high contents of initial common lead, but less than Itambé sample, and reverse discordance. The U content is at least ten times smaller than the Itambé sample, but the proportion of radiogenic Pb relative to the initial Pb is very high, thus the ages were not greatly affected by the presence of initial common lead. The ID-TIMS results also shows a good agreement with the results of LA-Q-ICP-MS and LA-SF-ICP-MS geochronology.

Despite the reverse discordancy observed in the TIMS data for monazite from Itambé and Bananeira (this study) and other "Moacyr/Moacir" monazite in the literature (e.g. Gasquet et al., 2010; Palin et al., 2013), the lower precision of the various LA-ICP-MS techniques, compared to TIMS, yields U–Pb isotope data for these monazites, when analysed as unknowns, that are concordant (Tables 6 and 7). Moreover, the LA-ICP-MS data is in agreement to their TIMS crystallization ($^{207}Pb^*/^{235}U$) age (this study; Cabral and Zeh, 2015). This suggests that these monazites can be used successfully as secondary reference materials for high-spatial resolution U–Pb geochronology. The question remains about their suitability as primary U–Pb reference reference materials for LA-ICP-MS (e.g. Gasquet et al., 2010; Palin et al., 2013) or SIMS (Harley and Nandakumar, 2014) techniques. In order to assess this for the monazite in this study, we have used the Bananeira monazite as the primary reference material for LA-SF-ICP-MS geochronology to date two U–Pb reference materials (USGS 44069, Thompson Mine monazite) as well as monazite from Steenkampskraal (South Africa), for which there are previously published SHRIMP and LA-ICP-MS ages. For data reduction of the unknowns, it was assumed that the Bannaneira reference material had the average of the isotope ratios obtained from the seven splits by ID-TIMS ($^{207}Pb^*/^{235}U$ = 0.6487, $^{206}Pb^*/^{238}U$ = 0.08294 and $^{207}Pb^*/^{206}Pb^*$ = 0.056723). The use of the common led-corrected ratios to the standardize unknowns has been used in several LA-ICP-MS studies, including other reference material development (e.g., Nasdala et al., 2008, Sláma et al., 2008, Jackson et al., 2004). Data reduction were performed using the Glitter 4.4.3 (Van Achterbergh et al., 2001).

Eighteen spot analyses of the USGS 44069 monazite (TIMS age: 424.9 ± 0.4 Ma; Aleinikoff et al., 2006) resulted in a weighted average $^{207}Pb^*/^{235}U$, $^{206}Pb^*/^{238}U$ and $^{207}Pb^*/^{206}Pb^*$ ages of 426 ± 5.1 Ma (95% c.l.; MSWD = 0.58), 426.3 ± 5.1 Ma (95% c.l.; MSWD = 1.6) and 430 ± 19.4 Ma (95% c.l.; MSWD = 0.22), respectively (Table 11 and Fig. 13). These ages are in complete agreement with the previous ID-TIMS and LA-ICP-MS data published for this monazite (e.g., Aleinikoff et al., 2006; Tollo et al., 2006; Gerbi and West, 2007; Alagna et al., 2008; Pullen et al., 2008; Liu et al., 2012). In addition, 18 analyses were obtained from the Thompson Mine monazite reference material

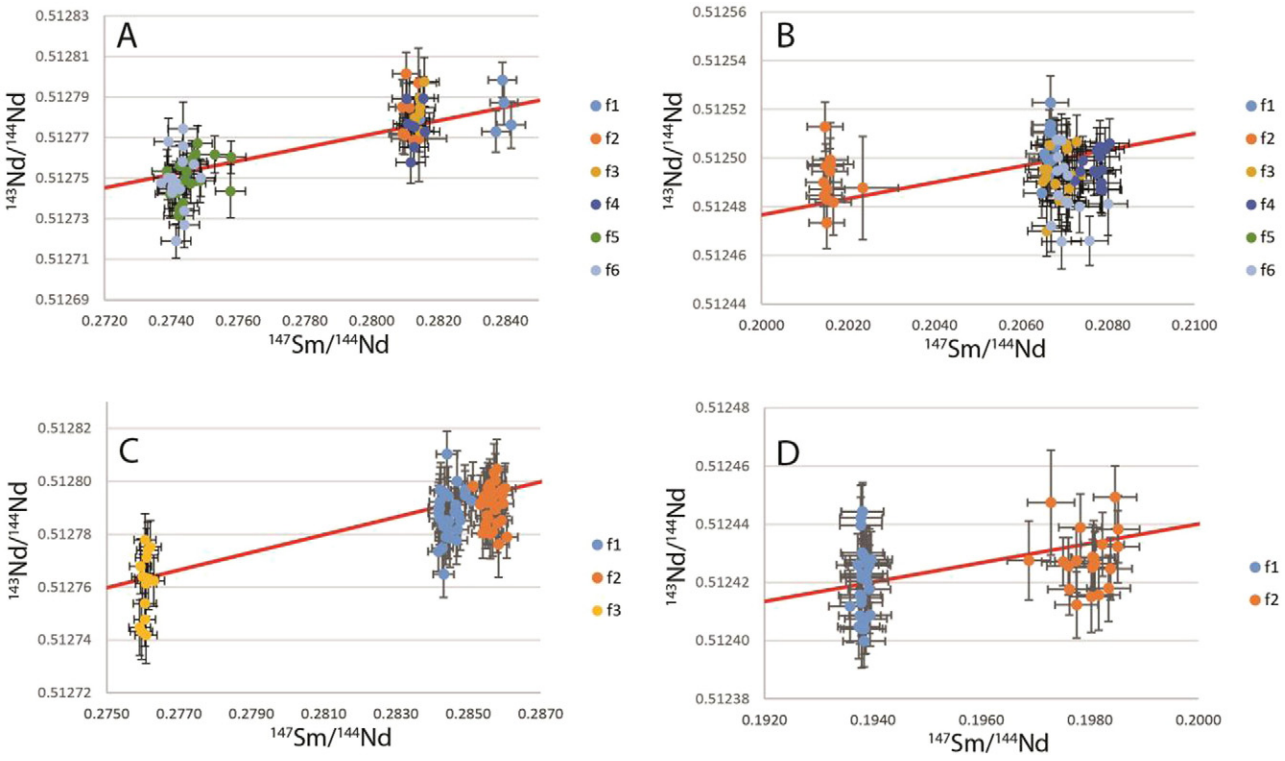

Fig. 9. Sm–Nd isotopic values for the Brazilian monazite samples in this study, using NIST610 as the reference material. (A) Bananeira, (B) Coqueiro, (C) Paraíso and (D) Itambé. The reference isochron ages for the Itambé and Bananeira samples are based on the ID-TIMS data from this study. The reference isochron ages for the Coqueiro and Paraíso are based on the LA-SF-ICP-MS data from this study. Error bars are 2σ.

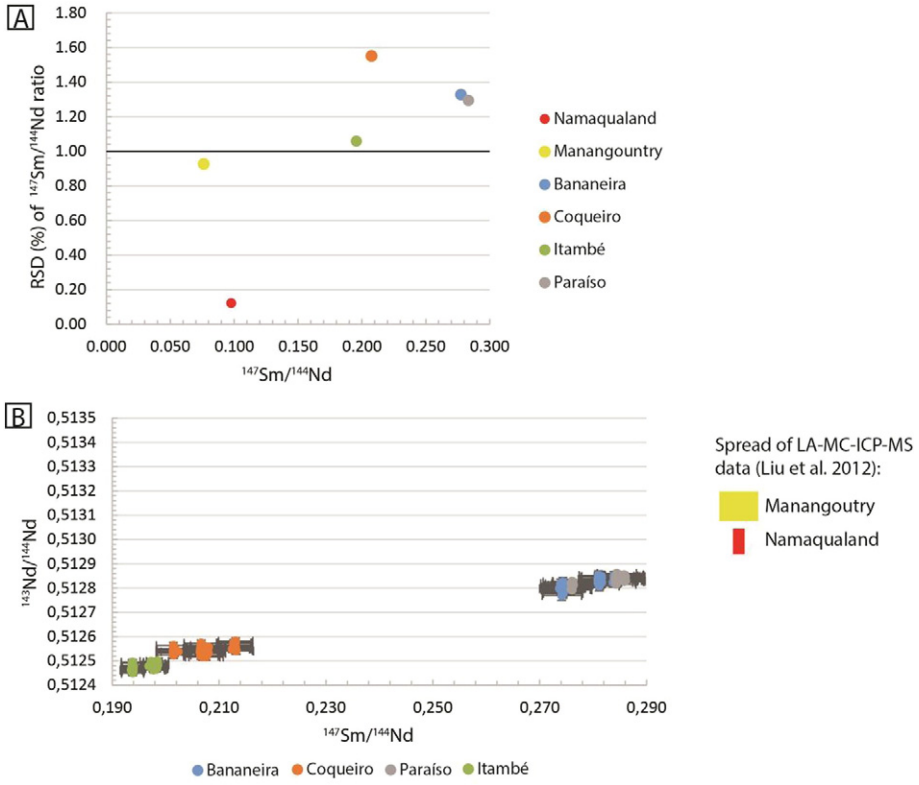

Fig. 10. A — Variations in $^{147}Sm/^{144}Nd$ for the studied monazites and references monazites (Namaqualand and Managountry data from Liu et al., 2012). Relative reference material deviation (RSD%) is used to measure the range of variations in the $^{147}Sm/^{144}Nd$ ratio. B — $^{143}Nd/^{144}Nd$ vs. $^{147}Sm/^{144}Nd$ plot to compare the uniformity of the Sm–Nd isotope compositions of the samples and reference materials from Liu et al. (2012). Error bars are reference material deviations (SD).

Table 10
Sm–Nd isotopic compositions of the Itambé sample determined by LA-MC-ICP-MS normalized both for NIST610 and Steenkampskral monazite.

Sample	Grain	Nd_{tot} (V)	$^{147}Sm/^{144}Nd$[b]	±2σ	βSm[c]	βNd[c]	$^{145}Nd/^{144}Nd$[d]	$^{148}Nd/^{144}Nd$[d]	$^{150}Nd/^{144}Nd$[d]	$^{143}Nd/^{144}Nd$[d]	±2σ	$^{143}Nd/^{144}Nd_i$[e]	εNd $_i$[e]	±2σ
Itambé (NIST610)	1 (n = 29)	45.6	0.1938	0.0004	−1.58	−1.78	0.348403	0.241563	0.237369	0.512421	0.000011	0.511777	−4.1	0.4
	2 (n = 20)	48.4	0.1980	0.0004	−1.59	−1.79	0.348400	0.241569	0.237026	0.512428	0.000011	0.51177	−4.2	0.4
Itambé (Steenkampskral)	1 (n = 20)	22.6	0.2007	0.0004	−1.08	−1.28	0.348410	0.241539	0.237414	0.512465	0.000012	0.511797	−3.7	0.4
	2 (n = 15)	16.7	0.1993	0.0004	−1.22	−1.43	0.348414	0.241544	0.237698	0.512462	0.000014	0.511799	−3.6	0.5

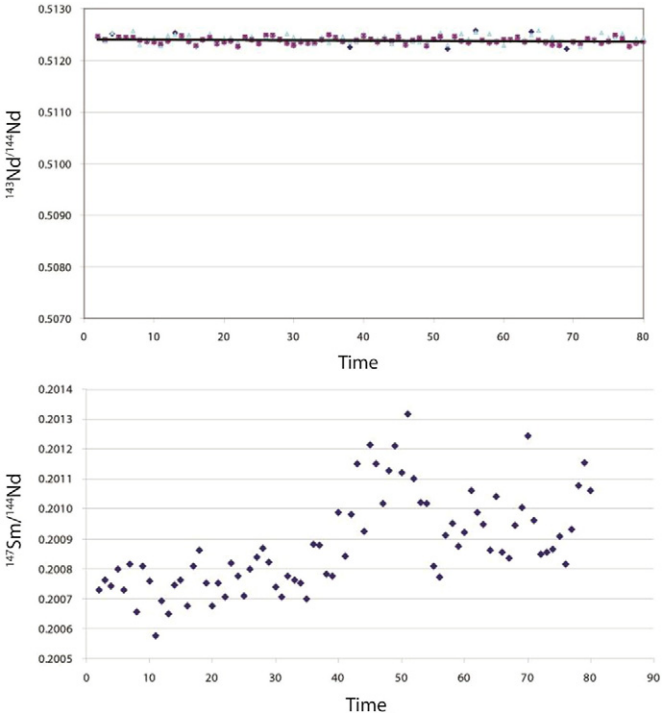

Fig. 11. Time-resolved pattern of the $^{143}Nd/^{144}Nd$ and $^{147}Sm/^{144}Nd$ of the Itambé monazite.

(Williams et al., 1996). These analyses yielded a concordia age of 1761.2 ± 17.2 Ma (2σ; MSWD of concordance and equivalence = 0.15, Fig. 13) and weighted average $^{207}Pb^*/^{235}U$ age of 1760.6 ± 17.9 Ma (95% c.l.; MSWD = 0.35, Table 11). The ages are in generally good agreement with the assumed age of 1766 Ma (Williams et al., 1996), for which analytical uncertainties have never been published.

Lastly, 13 analyses were obtained from Steenkampskraal monazite (or Namaqualand monazite, Liu et al., 2012). The LA-SF-ICP-MS analyses yielded a concordia age of 1034.4 ± 5.8 Ma (2σ; MSWD of concordance and equivalence = 0.15, Fig. 13), and weighted average $^{207}Pb^*/^{235}U$ age of 1034.4 ± 5.8 Ma (95% c.l.; MSWD = 0.22; Table 11). These results agree with a ca. 1033 Ma SHRIMP age of Knoper et al. (2000), and an unpublished SHRIMP U–Pb concordia age of 1030.4 ± 6.1 Ma (95% c.l.) using USGS 44069 monazite as the primary calibration reference material (Buick, unpublished data).

The results of the round-robin analysis using Bananeira monazite as primary reference material demonstrates its suitability as a primary reference material for U–Pb geochronology by LA-ICP-MS. The other samples from the Itambé district, Coqueiro and Paraíso monazites, have within error, the same age LA-(Q and SF)-ICP-MS ages as the Itambé and Bananeira samples (Fig. 12). That suggests the possibility of their use as, at least, a secondary reference material as well.

5.2. Sm–Nd reference material evaluation

The requirements for a mineral to serve as a Sm–Nd isotopic reference material includes that: it matrix matches the unknowns to be analysed; it has homogeneous $^{143}Nd/^{144}Nd$ and $^{147}Sm/^{144}Nd$ compositions; and that it is available in large quantities of coarse-grained, gem-quality crystals for distribution.

The influence of a matrix effect on $^{147}Sm/^{144}Nd$ fractionation during LA-MC-ICP-MS analysis is controversial. Iizuka et al. (2011) has observed a significant difference in the fractionation of $^{147}Sm/^{144}Nd$ between monazite and NIST glass in the same analytical session. Fisher et al. (2011), on the other hand, presented a highly correlated $\beta_{(Sm)}$–$\beta_{(Nd)}$ for different matrices, therefore no matrix effect was

Table 11
LA-SF-ICP-MS results for the round-robin analysis using Bananeira monazite as primary reference material. See caption of Table 7 for more information.

Sample	Pb207[a] (cps)	$^{206}Pb/^{204}Pb$	$^{206}Pb/^{238}U$[b]	±2σ (abs)	$^{207}Pb/^{235}U$[b]	±2σ (abs)	$^{208}Pb/^{232}Th$[b]	±2σ (abs)	$^{207}Pb/^{206}Pb$[b]	±2σ (abs)	rho[c]	$^{206}Pb/^{238}U$	±2σ (Ma)	$^{207}Pb/^{235}U$	±2σ (Ma)	$^{208}Pb/^{232}Th$	±2σ (Ma)	$^{207}Pb/^{206}Pb$	±2σ (Ma)
44069 (n = 18)	2293	14493	0.06840	0.00153	0.52294	0.01946	0.02676	0.00060	0.05547	0.00216	0.61	427	9	427	13	537	12	431	85
SD	470.5	17295.2	0.00095	0.00009	0.00753	0.00337	0.00300	0.00009	0.00046	0.00038	0.08	5.7	0.5	5.0	2.2	61.3	1.7	18.7	14.5
RSD%	20.5	119.3	1.4	5.7	1.4	17.3	11.2	14.4	0.8	17.4	12.5	1.3	5.8	1.2	17.2	11.4	13.8	4.3	17.1
Thompson Mine (n = 18)	9662	29679	0.31587	0.00675	4.66442	0.13588	0.09787	0.08312	0.10713	0.00326	0.74	1770	33	1761	24	1773	37	1751	55
SD	1357.2	42527.8	0.00102	0.00023	0.04185	0.01335	0.00825	0.09348	0.00097	0.00033	0.04	5.0	1.1	7.5	2.3	54.4	2.7	16.6	5.3
RSD%	14.0	143.3	0.3	3.4	0.9	9.8	8.4	112.5	0.9	10.0	6.1	0.3	3.4	0.4	9.5	3.1	7.5	0.9	9.7
Steenkampskraal (n = 13)	4680	34645	0.17411	0.00361	1.76935	0.05033	0.04869	0.00096	0.07374	0.00221	0.74	1035	20	1034	18	960	19	1034	60
SD	383.3	31332.6	0.00069	0.00020	0.01081	0.00795	0.00047	0.00003	0.00024	0.00034	0.07	3.7	1.1	4.0	2.9	9.3	0.6	6.7	9.1
RSD%	8.2	90.4	0.4	5.5	0.6	15.8	1.0	3.1	0.3	15.5	9.4	0.4	5.5	0.4	15.8	1.0	3.3	0.6	15.3

observed on the Sm–Nd mass bias, implying no need to use a matrix-match reference material as an external reference material. In contrast, Liu et al. (2012) observed differences in the $^{147}Sm/^{144}Nd$ correction factors for monazite, LREE glass and apatite, showing a significant matrix effect even though the materials had similar relationship between $\beta_{(Sm)}$ and $\beta_{(Nd)}$.

In order to evaluate possible matrix effects, in this study a first set of analyses of all the Brazilian samples were undertaken using NIST 610 synthetic glass as the reference material. For comparison, another dataset was collected from the Itambé monazite alone, using the proposed Namaqualand (Steenkampskraal) monazite Nd-isotope reference material (Liu et al., 2012). For Itambé the isotope data were the same, within error, regardless the reference material used, suggesting that use of the NIST glass reference material did not introduce a significant matrix effect.

As shown on Table 9 and Figs. 9 and 10, the monazites from this study have slight grain-scale variations in $^{147}Sm/^{144}Nd$ and, to a much smaller extent, $^{143}Nd/^{144}Nd$ isotopic ratios. The magnitude of NIST610-reference materialized heterogeneity of the $^{147}Sm/^{144}Nd$ isotopic composition of the Bananeira, Coqueiro and Paraíso are similar, and cannot be related to down-hole fractionation. In the other hand, the Itambé sample is more isotopically homogeneous, and comparable to the Managountry Nd-isotope reference material (Liu et al., 2012; Fig. 10). Although further investigations needs to be undertaken (solution MC-ICP-MS and/or ID-TIMS), the Itambé monazite has potential as reference material for Sm–Nd analysis by LA-MC-ICP-MS.

5.3. Trace element reference material evaluation

As already noted, the Bananeira monazite has been previously used as a primary reference material for monazite major and trace element chemistry by Kylander-Clark et al. (2013). According to our results (Table 5 and Fig. 5), the Bananeira, Coqueiro and Paraíso monazites have homogeneous compositions, implying their suitability as concentrations reference materials. Even though the Bananeira monazite has been previously used as concentration reference material, our results showed that the Coqueiro sample is the most homogeneous monazite with the RSD%, in general, lower than 1–2%, comparable to the NIST612 synthetic glass for some elements (Table 5), and below the

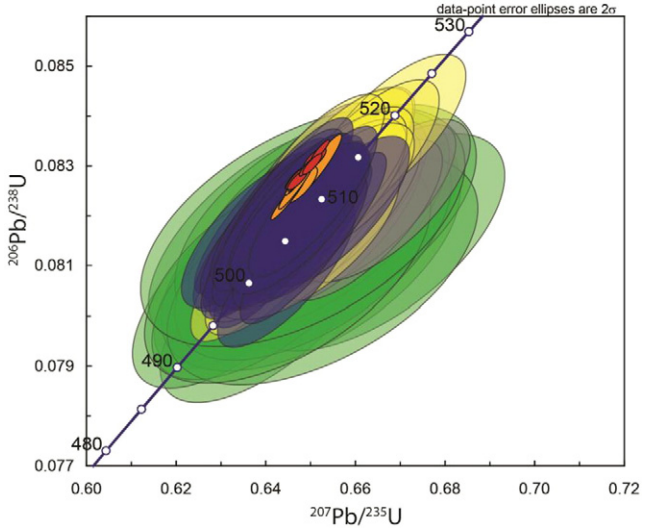

Fig. 12. Compilation of the LA-SF-ICP-MS and ID-TIMS results showing that, despite the reverse discordance of the ID-TIMS results, the lower precision of the LA-ICP-MS technique yields concordant results that agrees, within error, to the ID-TIMS ages. Green ellipses — Bananeira; grey — Coqueiro, yellow — Paraíso and blue — Itambé. Red and orange filled ellipses are Bananeira and Itambé ID-TIMS results, respectively.

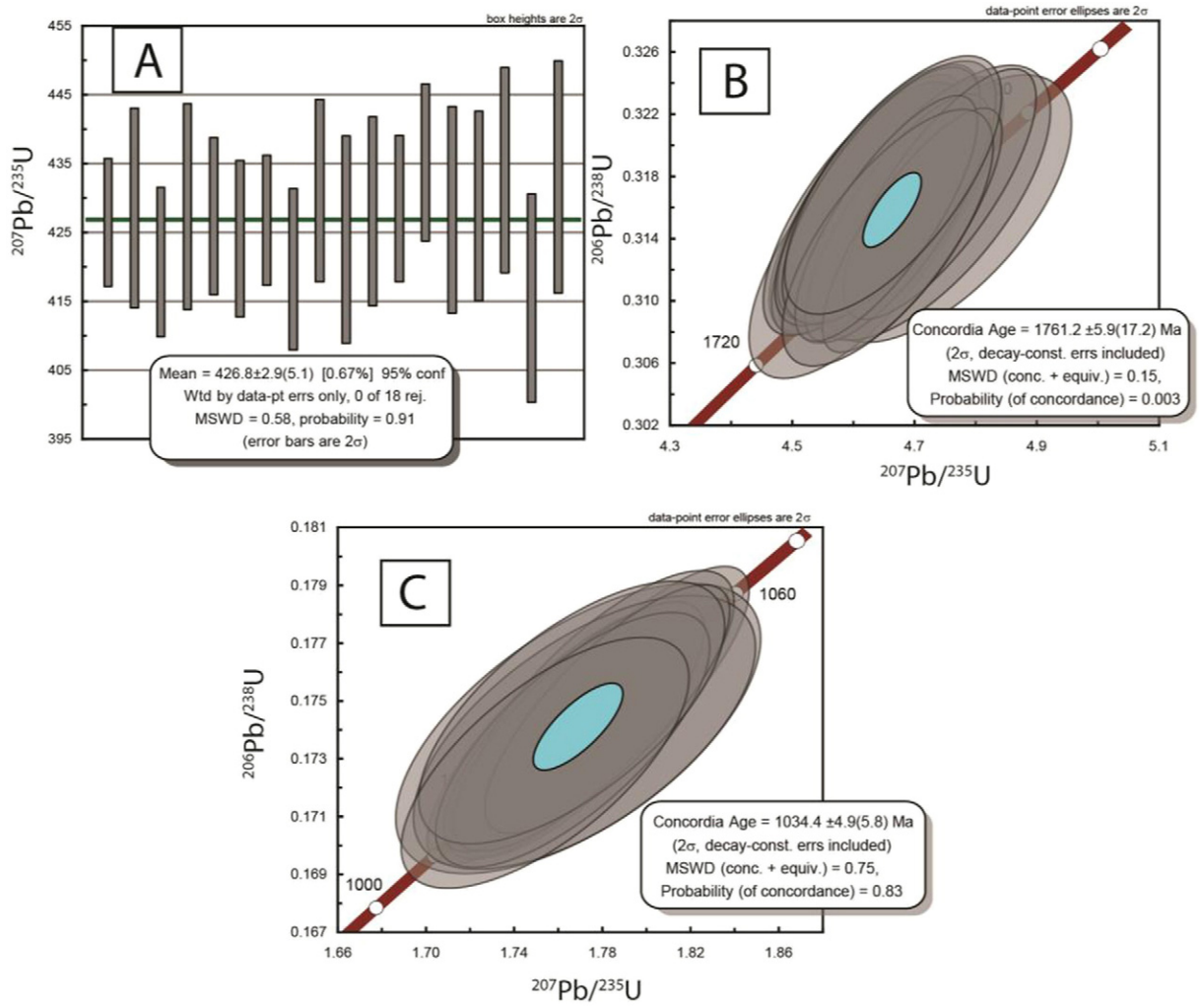

Fig. 13. Known reference materials analysed as unknowns using Bananeira monazite as primary reference material by LA-SF-ICP-MS. A - 44,069 monazite, B - Thompson mine monazite, C - Steenkampskrall monazite.

5% that is the maximum variation that is expected for a reference material for trace elements analysis.

5.4. Origin of "Moacyr" monazite

Monazite from the Itambé pegmatite district of Bahia state (Brazil) has been used as a primary reference material in a number of U–Pb studies. The initial TIMS age for this material is 474 ± 1 Ma (Seydoux-Guillaume et al., 2002, Paquette and Tiepolo, 2007). However, subsequently reported TIMS age (quoted as $^{207}Pb/^{235}U$ due to minor reverse discordance) of 504 ± 0.2 Ma (Gasquet et al., 2010) and 506 ± 1 Ma (Dumond et al., 2008) are available. None of the latter groups of ages agrees with the Seydoux-Guillaume et al. (2002) and the latter group themselves do not appear to wholly agree within stated uncertainties.

As the "Moacyr" monazite is of excellent quality and is used as a primary or secondary reference material in many laboratories it is also important to determine the reasons for disparity between the 504–510 Ma ages. However, there is no basic description of the source pegmatite, or the chemical composition of the samples in the literature. As result, in this paper we have evaluated monazites from three different pegmatite bodies from the Itambé district (Bananeira, Coqueiro and Paraíso) and compared it to an aliquot of the "Moacyr" monazite itself in order to evaluate the source of the reference material. The U–Pb LA-ICP-MS results showed that the samples have, within precision of the technique, the same ages, so other means must be used to distinguish between them.

In regard to chemical composition (Table 5), on the basis of MREE/HREE fractionation (ie, $(La/Gd)_N$ and $(Gd/Lu)_N$ values), Eu/Eu* and the chondrite-normalized REE patterns of the Itambé monazite is very similar to that from the Coqueiro pegmatite, and both are distinctly different from the Bananeira and Paraíso monazites (Fig. 5). This distinction also is apparent in the Nd-isotope compositions, where the Itambé monazite overlaps in composition with that from Coqueiro, but not monazite from Bananeira or Paraiso. In investigating the origin of other pieces of "Moacyr/Moacir" monazite, and potential disagreement in accepted TIMS ages for this material in the literature, the combination of tracing by elemental and Nd-isotopic compositions appears to offer the best hope of identifying the original source pegmatite.

Lastly, the large number of pegmatites in the EBPP offer promise for the future development of other monazite reference materials of similar age to those from this study. As shown by Rubatto et al. (2014), the Itambé monazite has an unusual, very low oxygen isotope composition for monazite crystallized from a pegmatite source (bulk reference value = +0.46 ± 0.20‰, V-SMOW). It appears that the Nd-isotope composition of the monazites in this study also sets them apart from those from other EBPP pegmatites. Pegmatites from the Itambé pegmatite district sit in the São Francisco craton and their monazites (this study) have much less evolved Nd isotopic compositions (εNdi between −2.7 and −4.2) than those from EBPP pegmatites of similar

(c. 490–510 Ma) crystallization age to the south, which are situated in the Aracuai orogen itself. The latter monazites have εNdi in the range ~ −17 to −14 (Buick and Lana, unpublished data), with their origin being interpreted as the final stage of fractional crystallization of the wide-spread granitoid rocks of the area (Pedrosa-Soares et al., 2011). We, in the other hand, interpret the origin of the pegmatites of the Itambé district as related to the anataxis of the gnaisse-migmatitic basement of the São Francisco craton (Fig. 2). Also, the different εNdi values of the monazites can provide a further distinction for tracing Brazillian gem-quality monazite reference materials of aproximally the same age.

6. Conclusions

1) The combination of elemental and Sm–Nd isotopic compositions allowed the inference that the origin of the "Moacyr" monazite is from the Coqueiro pegmatite, from the Itambé district.
2) We propose the Bananeira monazite as a primary reference material for U–Pb LA-ICP-MS analyses, as the LA-ICP-MS results agrees, within error, to the ID-TIMS results. Furthermore, it was possible to reproduce the ages of others known reference materials, using it as primary reference material. The best estimative for Bananeira's crystallization age ($^{207}Pb^*/^{235}U$) is 507.7 ± 1.3 Ma (95% c.l.; MSWD = 6.8) and an average Th/U ratio of 27.6.
3) Our results also show the suitability for the other monazites from the Itambé district as, at least, secondary reference material for U–Pb LA-ICP-MS analysis.
4) The very homogeneous REE results of the Coqueiro monazite indicates its potential as a natural reference material for trace elements analyses for LA-Q-ICP-MS.
5) Furthermore, the variations between the "Moacyr" monazite of the literature and our Itambé sample may suggest a thorough characterization and evaluation of the chemical and isotopic signatures of individual portions of megacrystals prior to their use in a given laboratory.
6) Lastly, the εNd is an adequate tool for tracing Brazillian gem-quality monazite reference materials, apart from the approximately 505 Ma age.

We are willing to distribute those reference materials upon request to other laboratories.

Acknowledgments

The first author acknowledges CNPq for providing the masters scholarship (134179/2013-7) and FAPEMIG-VALE CRA RDP-00063/10, FINEP CT-INFRA, FAPEMIG (APQ03943; RDP 0067-10) and CNPQ (402852/2012-5; 401334/2012-0; 302633/2011-1) projects for financial support. ISB acknowledges support from the "Programa Ciência Sem Fronteiras/Science Without Borders Program" (CNPq; Brazil), and the National Research Foundation (NRF, South Africa). We also acknowledge editor Klaus Mezger, Chris Fisher and an anonymous referee for comments and suggestions.

Appendix A. Supplementary data

Supplementary data to this article can be found online at http://dx.doi.org/10.1016/j.chemgeo.2015.12.019.

References

Alagna, K.E., Petrelli, M., Perugini, D., Poli, G., 2008. Micro-analytical zircon and monazite U–Pb isotope dating by laser ablation inductively coupled plasma-quadrupole mass spectrometry. Geostand. Geoanal. Res. 32, 103–120.
Aleinikoff, J.N., Schenk, W.S., Plank, M.O., Srogi, L.A., Fanning, C.M., Kamo, S.L., Bosbyshell, H., 2006. Deciphering igneous and metamorphic events in high-grade rocks of the Wilmington complex, Delaware: morphology, cathodoluminescence and backscattered electron zoning, and SHRIMP U–Pb geochronology of zircon and monazite. Geol. Soc. Am. Bull. 118, 39–64.
Back, M.E., Mandarino, J.A., 2008. Mineral Species. first ed The Mineral Record Inc., Tucson (345 pp.).
Bowie, S.H.U., Horne, J.E.T., 1953. Cheralite, a new mineral of the monazite group. Mineral. Mag. 30, 93–99.
Buick, I.S., Clark, C., Rubatto, D., Hermann, J., Pandit, M., Hand, M., 2010. Constraints on the Proterozoic evolution of the Aravalli-Delhi Orogenic belt (NW India) from monazite geochronology and mineral trace element geochemistry. Lithos 120, 511–520.
Cabral, A.R., Zeh, A., 2015. Detrital zircon without detritus: a result of 496-Ma-old fluid–rock interaction during the gold-lode formation of Passagem, Minas Gerais, Brazil. Lithos 212–215, 415–427. http://dx.doi.org/10.1016/j.lithos.2014.10.011.
Catlos, E.J., Gilley, L.D., Harrison, T.M., 2002. Interpretation of monazite ages obtained via in situ analysis. Chem. Geol. 188, 193–215.
Cherniak, D.J., Watson, E.B., Grove, M., Harrison, T.M., 2004. Pb diffusion in monazite: a combined RBS/SIMS study. Geochim. Cosmochim. Acta 68, 829–840.
Cruz, M.J., Merlet, C., Sabaté, P., 1966. Datação pontual das monazitas da região de Itambé, Bahia, através da microssonda eletrônica. XXXIX Congresso Brasileiro de Geologia, Salvador, Brazil, Event Annals 2, pp. 206–209.
Della Ventura, G., Mottana, A., Parodi, G.C., Raudsepp, M., Bellatreccia, F., Caprilli, E., Rossi, P., Fiori, S., 1996. Monazite-huttonite solid-solutions from the Vico Volcanic Complex, Latium, Italy. Mineral. Mag. 60, 751–758.
DePaolo, D.J., 1988. Neodymium Isotope Geochemistry: An Introduction. Springer, Berlin.
Dumond, G., McLean, N., Williams, M.L., Jercinovic, M.J., Bowring, S.A., 2008. High-resolution dating of granite petrogenesis and deformation in a lower crustal shear zone; Athabasca granulite terrane, western Canadian Shield. Chem. Geol. 254, 197–215.
Fisher, C.M., McFarlane, C.R.M., Hanchar, J.M., Schmitz, M.D., Sylvester, P.J., Lam, R., Longerich, H.P., 2011. Sm–Nd isotope systematics by laser ablation-multicollector-inductively coupled plasma mass spectrometry: methods and potential natural and synthetic reference materials. Chem. Geol. 284, 1–20.
Fletcher, I.R., Davis, W.J., Rayner, N., Orestes, S.J., 2012. The Moacyr monazite standard: identity and compositional complications. 6th International SHRIMP Workshop, Canberra, Australia, Event Annals 1, pp. 49–51.
Förster, H.-J., 1998. The chemical composition of REE-Y-Th-U-rich accessory minerals in peraluminous granites of the Erzgebirge-Fichtelgebirge region, Germany. Part I: the monazite-(Ce)-brabantite solid solution series. Am. Mineral. 83, 259–272.
Förster, H.-J., Harlov, D.E., 1999. Monazite-(Ce)-huttonite solid solutions in granulite-facies metabasites from the Ivrea-Verbano Zone, Italy. Mineral. Mag. 64 (4), 587–594.
Foster, G., Kinny, P., Vance, D., Prince, C., Harris, N., 2000. The significance of monazite U–Th–Pb age data in metamorphic assemblages; a combined study of monazite and garnet chronometry. Earth Planet. Sci. Lett. 181, 327–340.
Foster, G., Gibson, H.D., Parrish, R., Horstwood, M., Fraser, J., Tindle, A., 2002. Textural, chemical and isotopic insights into the nature and behaviour of metamorphic monazite. Chem. Geol. 191, 183–207.
Franz, G., Andrehs, G., Rhede, D., 1996. Crystal chemistry of monazite and xenotime from Saxothuringian-Moldanubian metapelites, NE Bavaria, Germany. Eur. J. Mineral. 8, 1097–1108.
Gardes, E., Jaoul, O., Montel, J.M., Seydoux-Guillaume, A.M., Wirth, R., 2006. Pb diffusion in monazite: an experimental study of $Pb^{2+}+Th^{4+} \leftrightarrow 2Nd^{3+}$ interdiffusion. Geochim. Cosmochim. Acta 70, 2325–2336.
Gasquet, D., Bertrand, J.-M., Paquette, J.-L., Lehmann, J., Ratzov, G., De Ascenção Guedes, R., Tiepolo, M., Bollier, A.-M., Scaillet, S., Nomade, S., 2010. Miocene to Messinian deformation and hydrothermal activity in a pre-Alpine basement massif of the French western Alps: new U–Th–Pb and argon ages from the Lauzière massif. Bull. Geol. Soc. Fr. 181, 227–241.
Gehrels, G.E., Valencia, V.A., Ruiz, J., 2008. Enhanced precision, accuracy, efficiency, and spatial resolution of U–Pb ages by laser ablation-multicollector-inductively coupled plasma-mass spectrometry. Geochem. Geophys. Geosyst. 9, Q03017. http://dx.doi.org/10.1029/2007GC001805.
Gerbi, C., West Jr., D.P., 2007. Use of U–Pb geochronology to identify successive, spatially overlapping tectonic episodes during Silurian–Devonian orogenesis in south-central Maine, USA. Geol. Soc. Am. Bull. 119, 1218–1231.
Gerdes, A., Zeh, A., 2006. Combined U–Pb and Hf isotope LA-(MC-)ICP-MS analyses of detrital zircons: comparison with SHRIMP and new constraints for the provenance and age of an Armorican metasediment in Central Germany. Earth Planet. Sci. Lett. 249, 47–61.
Gerdes, A., Zeh, A., 2009. Zircon formation versus zircon alteration — new insights from combined U–Pb and Lu–Hf in-situ LA-ICP-MS analyses, and consequences for the interpretation of Archean zircon from the Central Zone of the Limpopo Belt. Chem. Geol. 261, 230–243.
Goudie, D., Fisher, C., Hanchar, J.M., Crowley, J.L., Ayers, J.C., 2014. Simultaneous in situ determination of U–Pb and Sm–Nd isotopes inmonazite by laser ablation ICP-MS. Geochem. Geophys. Geosyst. 15. http://dx.doi.org/10.1002/2014GC005431.
Gregory, C.J., McFarlane, C.R.M., Hermann, J., Rubatto, D., 2009. Tracing the evolution of calc-alkaline magmas: in-situ Sm–Nd isotope studies of accessory minerals in the Bergell Igneous Complex, Italy. Chem. Geol. 260, 73–86.
Hammerli, J., Kemp, A.I.S., Spandler, C., 2014. Neodymium isotope equilibration during crustal metamorphism revealed by in situ microanalysis of REE-rich accessory minerals. Earth Planet. Sci. Lett. 392, 133–142.
Harley, S.L., Nandakumar, V., 2014. Accessory Mineral Behaviour in Granulite Migmatites: a Case Study from the Kerala Khondalite Belt, India. J. Petrol. 55, 1965–2002. http://dx.doi.org/10.1093/petrology/egu047.
Harlov, D.E., Wirth, R., Hetherington, C.J., 2011. Fluid-mediated partial alteration in monazite: the role of coupled dissolutionreprecipitation in element redistribution and mass transfer. Contrib. Mineral. Petrol. 162, 329–348.
Harrison, T.M., McKeegan, K.D., Le Fort, P., 1995. Detection of inherited monazite in the Manaslu leucogranite by 208Pb/232Th ion microprobe dating: crystallization age and tectonic implications. Earth Planet. Sci. Lett. 133, 271–282.
Harrison, T.M., Catlos, E.J., Montel, J.M., 2002. U–Th–Pb dating of phosphate minerals. Phosphates Geochem. Geobiol. Mater. Importance 48, 523–558.
Hawkins, D.P., Bowring, S.A., 1997. U–Pb systematics of monazite and xenotime: case studies from the Paleoproterozoic of the Grand Canyon, Arizona. Contrib. Mineral. Petrol. 127, 87–103.
Heaman, L., Parrish, R., 1991. U–Pb geochronology of accessory minerals. In: Heaman, L., Ludden, J.N. (Eds.), Applications of Radiogenic Isotope Systems to Problems in Geology, Short Course Handb 19. Mineral. Assoc. of Canada, Quebec, QC, Canada, pp. 59–102.
Horstwood, M.S.A., Foster, G.L., Parrish, R.R., Noble, S.R., Nowell, G.M., 2003. Common-Pb corrected in situ U–Pb accessory mineral geochronology by LA-MC-ICP-MS. J. Anal. At. Spectrom. 18, 837–846.

Iizuka, T., Eggins, S.M., McCulloch, M.T., Kinsley, L.P.J., Mortimer, G.E., 2011. Precise and accurate determination of Sm–147/Nd-144 and Nd-143/Nd-144 in monazite using laser ablation-MC-ICPMS. Chem. Geol. 282, 45–57.

Jackson, S.E., Pearson, N.J., Griffin, W.L., Belousova, E.A., 2004. The application of laser ablation-inductively coupled plasma-mass spectrometry to in situ U–Pb zircon geochronology. Chem. Geol. 211, 47–69.

Knoper, M., Armstrong, R.A., Andreoli, M.A.G., Ashwal, L.D., 2000. The Steenkampskraal monazite vein: a subhorizontal stretching shear zone indicating extensional collapse of Namaqualand at 1033 Ma? J. Afr. Earth Sci. 31, 38–39.

Kohn, M.J., Vervoort, J.D., 2008. U–Th–Pb dating of monazite by single-collector ICP-MS: pitfalls and potential. Geochem. Geophys. Geosyst. 9, Q04031. http://dx.doi.org/10.1029/2007GC001899.

Kosler, J., Tubrett, M.N., Sylvester, P.J., 2001. Application of laser ablation ICP-MS to U–Th–Pb dating of monazite. Geostand. Newslett. 25, 375–386.

Kylander-Clark, A.R.C., Hacker, B.R., Cottle, J.M., 2013. Laser-ablation split-stream ICP petrochronology. Chem. Geol. 345, 99–112. http://dx.doi.org/10.1016/j.chemgeo.2013.02.019.

Liu, Z.C., Wu, F.Y., Yang, Y.H., Yang, J.H., Wilde, S.A., 2012. Neodymium isotopic compositions of the standard monazites used in U–Th–Pb geochronology. Chem. Geol. 334, 221–239.

Machado, N., Gauthier, G., 1996. Determination of $^{207}Pb/^{206}Pb$ ages on zircon and monazite by laser ablation-ICPMS and application to a study of sedimentary provenance and metamorphism in southeastern Brazil. Geochim. Cosmochim. Acta 60, 5063–5073.

McFarlane, C.R.M., McCulloch, M.T., 2007. Coupling of *in-situ* Sm–Nd systematics and U–Pb dating of monazite and allanite with applications to crustal evolution studies. Chem. Geol. 245, 45–60.

Montel, J.M., Seydoux, A.M., 1998. Sm–Nd interdiffusion in monazite. 7th International Symposium on Experimental Mineralogy, Petrology and Geochemistry (Orléans 1998) 42.

Montel, J.M., Foret, S., Veschambre, M., Nicollet, C., Provost, A., 1996. Electron microprobe dating of monazite. Chem. Geol. 131, 37–53.

Nasdala, L., Hofmeister, W., Norberg, N., Mattinson, J.M., Corfu, F., Dörr, W., Kamo, S.L., Kennedy, A.K., Kronz, A., Reiners, P.W., Frei, D., Košler, J., Wan, Y., Götze, J., Häger, T., Kröner, A., Valley, J.W., 2008. Zircon M257 — a homogeneous natural reference material for the ion microprobe U–Pb analysis of zircon. Geostand. Geoanal. Res. 32, 247–265.

Ni, Y.X., Hughes, J.M., Mariano, A.N., 1995. Crystal-chemistry of the monazite and xenotime structures. Am. Mineral. 80, 21–26.

Palin, R.M., Searle, M.P., Waters, D.J., Parrish, R.R., Roberts, N.M.W., Horstwood, M.S.A., Yeh, M.-W., Chung, S.-L., Anh, T.T., 2013. A geochronological and petrological study of anatectic paragneiss and associatd granite dykes from Day Nui Con Voi metamorphic core complex, North Vietnam: constraints on the timing of metamorphism within the Red River shear zone. J. Metamorph. Geol. 31, 359–387. http://dx.doi.org/10.1111/jmg.12025.

Paquette, J.L., Tiepolo, M., 2007. High resolution (5 μm) U–Th–Pb isotope dating of monazite with excimer laser ablation (ELA)-ICPMS. Chem. Geol. 240, 222–237.

Paquette, J.-L., Nédélec, A., Moine, B., Rakotondrazafy, M., 1994. U–Pb, single zircon Pb-evaporation, and Sm–Nd isotopic study of a granulite domain in SE Madagascar. J. Geol. 102, 523–538.

Parrish, R.R., 1990. U–Pb Dating of Monazite and Its Application to Geological Problems. Can. J. Earth Sci. 27, 1431–1450.

Pedrosa-Soares, A.C., Noce, C.M., Wiedemann, C., Pinto, C.P., 2001. The Araçuaí-West-Congo Orogen in Brazil: an overview of a confined orogen formed during Gondwana land assembly. Precambrian Res. 110, 307–323.

Pedrosa-Soares, A.C., Alkmim, F.F., Tack, L., Noce, C.M., Babinski, M., Silva, L.C., Martins-Neto, M.A., 2008. Similarities and differences between the Brazilian and African counterparts of the Neoproterozoic Aracuai-West Congo orogen. West Gondwana: Pre-Cenozoic Correlations across the South Atlantic Region 294, pp. 153–172.

Pedrosa-Soares, A.C., De Campos, C.P., Noce, C., Silva, L.C., Novo, T., Roncato, J., Medeiros, S., Castaneda, C., Queiroga, G., Dantas, E., Dussin, I., Alkmim, F., 2011. Late Neoproterozoic-Cambrian granitic magmatism in the Aracuai orogen (Brazil), the Eastern Brazilian Pegmatite Province and related mineral resources. Granite-Relat. Ore Depos. 350, 25–51.

Poitrasson, F., Chenery, S., Shepherd, T.J., 2000. Electron microprobe and LA-ICP-MS study of monazite hydrothermal alteration: implications for U–Th–Pb geochronology and nuclear ceramics. Geochim. Cosmochim. Acta 64 (19), 3283–3297.

Pullen, A., Kapp, P., Gehrels, G.E., DeCelles, P.G., Brown, E.H., Fabijanic, J.M., Ding, L., 2008. Gangdese retroarc thrust belt and foreland basin deposits in the Damxung area, southern Tibet. J. Asian Earth Sci. 33, 323–336.

Pyle, J.M., Spear, F.S., Rudnick, R.L., McDonough, W.F., 2001. Monazite–Xenotime–Garnet Equilibrium in Metapelites and a New Monazite–Garnet Thermometer. J. Petrol. 42, 2083–2107.

Rapp, R.P., Watson, E.B., 1986. Monazite solubility and dissolution kinetics: implications for the thorium and light rare-earth chemistry of felsic magmas. Contrib. Mineral. Petrol. 94, 304–316.

Rubatto, D., Putlitz, B., Gauthiez-Putallaz, L., Crépisson, C., Buick, I.S., Zheng, Y., 2014. Measurement of in-situ oxygen isotope ratios inmonazite by SHRIMP ion microprobe: standards, protocols and implications. Chem. Geol. 380, 84–96. http://dx.doi.org/10.1016/j.chemgeo.2014.04.029.

Schärer, U., 1984. The effect of initial ^{230}Th disequilibrium on young U–Pb ages: the Makalu case, Himalaya. Earth Planet. Sci. Lett. 67, 191–204.

Seydoux-Guillaume, A.M., Montel, J.M., Paquette, J.L., Marinho, M., 1999. Experimental study of the resetting of the U–Th–Pb geochronological system of monazite. EUG X. Terra Nova 10 (Abstr Suppl. 1), 800.

Seydoux-Guillaume, A.M., Wirth, R., Nasdala, L., Gottschalk, M., Montel, J.M., Heinrich, W., 2002. An XRD, TEM and Raman study of experimentally annealed natural monazite. Phys. Chem. Miner. 29, 240–253.

Silva, E.F.A., Cunha, J.C., Marinho, M.M., 1996. Pegmatitos da região de Itambé, Bahia: geologia e potencialidade econômica. CBPM-Companhia Bahiana de Pesquisa Mineral. Série Arquivos Abertos 10 (41 pp.).

Sláma, J., Kosler, J., Condon, D.J., Crowley, J.L., Gerdes, A., Hanchar, J.M., Horstwood, M.S.A., Morris, G.A., Nasdala, L., Norberg, N., Schaltegger, U., Schoene, B., Tubrett, M.N., Whitehouse, M.J., 2008. Plešovice zircon - a new natural reference material for U–Pb and Hf isotopic microanalysis. Chem. Geol. 249, 1–35.

Stacey, J.S., Kramers, J.D., 1975. Approximate of terrestrial lead isotope variation by a two-stage model. Earth Planet. Sci. Lett. 26, 207–221.

Stepanov, A.S., Hermann, J., Rubatto, D., Rapp, R.P., 2012. Experimental study of monazite/melt partitioning with implications for the REE, Th and U geochemistry of crustal rocks. Chem. Geol. 300-301, 200–220.

Stern, R.A., Berman, R.G., 2001. Monazite U–Pb and Th–Pb geochronology by ion microprobe, with an application to in situ dating of an Archean metasedimentary rock. Chem. Geol. 172, 113–130.

Sun, S.-S., McDonough, W.F., 1989. Chemical and isotopic systematics of oceanic basalts: implications for mantle compositions and processes. In: Saunders, A.D., Norry, M.J. (Eds.), Magmatism in the ocean basins. Geological Society Special Publication 42, pp. 313–345.

Suzuki, K., Adachi, M., 1991. Precambrian provenance and Silurian metamorphism of the Tsunosawa paragneiss in the South Kitakami terrane, northeast Japan, revealed by the chemical Th-U-total Pb isochron ages of monazite, zircon and xenotime. J. Geochem. 25, 357–376.

Thöni, M., Miller, C., Zanetti, A., Habler, G., Goessler, W., 2008. Sm–Nd isotope systematics of high-REE accessory minerals and major phases: ID-TIMS, LA-ICP-MS and EPMA data constrain multiple Permian-Triassic pegmatite emplacement in the Koralpe, Eastern Alps. Chem. Geol. 254, 216–237.

Tollo, R.P., Aleinikoff, J.N., Borduas, E.A., Dickin, A.P., McNutt, R.H., Fanning, C.M., 2006. Grenvillian magmatism in the northern Virginia blue ridge: petrologic implications of episodic granitic magma production and the significance of postorogenic a-type charnockite. Precambrian Res. 151, 224–264.

Tomascak, P.B., Krogstad, E.J., Walker, R.J., 1998. Sm–Nd isotope systematics and the derivation of granitic pegmatites in southwestern Maine. Can. Mineral. 36, 327–337.

Van Achterbergh, E., Ryan, C.G., Jackson, S.E., Griffin, W.L., 2001. Data reduction software for LA-ICP-MS: appendix. Assoc. Canada (MAC) Short Course Series 29, p. 239.

Warren, C.J., Grujie, D., Kellett, D.A., Cottle, J., Jamieson, R.A., Ghalley, K.S., 2011. Probing the depth of the India-Asia collision: U–Th–Pb monazite chronology of granulites from NW Bhutan. Tectonics 30, TC2004. http://dx.doi.org/10.1029/2010TC002738.

Wasserburg, G.J., Jacousen, S.B., DePaolo, D.J., McCulloch, M.T., Wen, T., 1981. Precise determination of Sm/Nd ratios, Sm and Nd isotopic abundances in standard solutions. Geochim. Cosmochim. Acta 45, 2311–2323.

Williams, I.S., Buick, I.S., Cartwright, I., 1996. An extended episode of early Mesoproterozoic metamorphic fluid flow in the Reynolds range, central Australia. J. Metamorph. Geol. 14, 29–48.

Williams, M.L., Jercinovic, M.J., Hetherington, C.J., 2007. Microprobe monazite geochronology: understanding geologic processes by integrating composition and chronology. Annu. Rev. Earth Planet. Sci. 35, 137–175.

Williams, M.L., Jercinovic, M.J., Harlov, D.E., Budzyń, B., Hethington, C.J., 2011. Resetting monazite ages during fluid-related alteration. Chem. Geol. 283, 218–225. http://dx.doi.org/10.1016/j.chemgeo.2011.01.019.

Yang, Y.H., Sun, J.F., Xie, L.W., Fan, H.R., Wu, F.Y., 2008. In situ Nd isotopic measurement of natural geologic materials by LA-MC-ICPMS. Chin. Sci. Bull. 53, 1062–1070.